Quaternary Science Reviews 293 (2022) 107704

Contents lists available at ScienceDirect

Quaternary Science Reviews

journal homepage: www.elsevier.com/locate/quascirev

Deglacial to Mid Holocene environmental conditions on the northeastern Greenland shelf, western Fram Strait

Katrine Elnegaard Hansen [a, *], Jesper Lorenzen [a], Joanna Davies [a], Lukas Wacker [b], Christof Pearce [a], Marit-Solveig Seidenkrantz [a]

[a] Paleoceanography and Paleoclimate Group, Department of Geoscience, Arctic Research Centre and iClimate, Aarhus University, Høegh-Guldbergs Gade 2, 8000, Aarhus C, Denmark
[b] Laboratory of Ion Beam Physics, ETH, Otto-Stern-Weg 5, Zürich, CH-8093, Switzerland

ARTICLE INFO

Article history:
Received 24 February 2022
Received in revised form
3 August 2022
Accepted 4 August 2022
Available online xxx

Handling editor: Dr A. Voelker

Keywords:
Westwind Trough
Holocene
Greenland
Deglacial
Micropaleontology
Foraminifers
X-ray fluorescence
Grain size
Palaeoceanography

ABSTRACT

The western Fram Strait is the only deep-water gateway connecting the Arctic Ocean and North Atlantic. Consequently, today, the western Fram Strait and the Northeast Greenland shelf receive cold, low saline Polar and Arctic Atlantic waters from the Arctic Ocean incorporated in the East Greenland Current, together with warmer, saline recirculated Atlantic Water masses derived from the West Spitsbergen Current. We present a multiproxy study (grain size distribution, XRF core scans, and benthic foraminiferal assemblages) based on the lower part of the radiocarbon dated marine sediment core DA17-NG-ST03-039G, covering the period from 13.3 to 3.9 cal ka BP. We reconstruct the deglacial conditions of the Northeast Greenland shelf together with Early to Mid Holocene fluctuations in subsurface Atlantic Water and Polar Water advection. The results show that the outer Northeast Greenland shelf was deglaciated and marine conditions were established prior to c. 13.3 cal ka BP. At this time, our data show Atlantic Water masses flowing beneath an extensive sea-ice cover in a glaciomarine setting, potentially related to the Bølling-Allerød warm period. Around 12.9 cal ka BP, the onset of high surface and bottom water productivity may be associated with the Younger Dryas onset. This was followed by a transition towards warmer bottom and subsurface water conditions from c. 11.7 until 10.2 cal ka BP caused by enhanced advection of Atlantic-derived water masses. A cold period with marginal ice zone conditions and enhanced East Greenland Current incursion is evident from 10.2 to 9.4 cal ka BP, succeeded by harsher sea-ice conditions and Atlantic Water inflow, prevailing until c. 7.5 cal ka BP. Holocene Thermal Maximum conditions, characterized by high surface and subsurface water productivity, were promoted by enhanced Atlantic Water flow to the shelf from c. 7.5 to 6.7 cal ka BP. In contrast, the transition towards a cold period with increased drift-ice transport via a strong East Greenland Current is recorded from c. 6.2 cal ka BP and to the end of our record at 3.9 cal ka BP; it was associated with the onset of the Neoglaciation.

1. Introduction

The Fram Strait is one of the two main gateways connecting the Arctic Ocean to the North Atlantic. Via the Fram Strait, the East Greenland Current (EGC) conveys cold low-saline, Polar surface waters, together with glacial meltwater and drift ice along the eastern Greenland margin and into the North Atlantic. This freshwater flux from Greenland and the Arctic Ocean affects local marine ecosystems and glacier dynamics, as well as ocean and atmospheric temperatures (Rysgaard et al., 2003; Seale et al., 2011; Smith and Gregory, 2009). Furthermore, model studies have shown that increased export of freshwater to the convective sub-arctic deep-water formation regions have an immense impact on the Atlantic Meridional Overturning Circulation (AMOC) (Proshutinsky et al., 2002; Swingedouw et al., 2006). The AMOC acts as a key element in the global heat transport and distribution of water masses, including the northward advection of Atlantic Water masses to higher latitudes. A future warming of the Arctic Ocean will increase sea ice melting and consequently cause elevated propagation of freshwater into the North Atlantic via the Fram Strait. Additionally,

* Corresponding author. Katrine Elnegaard Hansen,
E-mail address: katrine.elnegaard@geo.au.dk (Katrine Elnegaard Hansen).

https://doi.org/10.1016/j.quascirev.2022.107704

a model simulation based on the IPCC RCP8.5 scenario has suggested the disappearance of Arctic summer sea-ice by 2100, and a decrease of the AMOC intensity of 72% by 2300 caused by the elevated freshwater export from the Arctic Ocean (Jahn and Holland, 2013). Accordingly, studying past relative variability of the EGC and Atlantic Water advection can aid in evaluating pre-industrial conditions and potentially further improve predictions of the future regional climate and AMOC sensitivity.

The past deglacial and Holocene climatic and oceanographic variability of the eastern Fram Strait and western Svalbard regions have been investigated intensively (e.g. Aagaard-Sørensen et al., 2014a; Müller and Stein, 2014; Rasmussen et al., 2007; Werner et al., 2013, 2016). In contrast, knowledge of past changes in sea ice, oceanography and climate based on sediment core analyses in the western Fram Strait and offshore Northeast Greenland is scarce, with only a few studies published so far (Davies et al., 2022; Pados-Dibattista et al., 2022; Spielhagen and Mackensen, 2021; Syring et al., 2020a, 2020b; Zehnich et al., 2020). The extent of the Greenland Ice Sheet (GIS) during the last glaciation also remains poorly constrained (Arndt et al., 2017; Evans et al., 2009; Funder et al., 2011b; Winkelmann et al., 2010) as only a few marine records from the Northeast Greenland shelf span this period.

Remarkably low sea-ice cover during September 2017 allowed the retrieval of several marine sediment cores from the Northeast Greenland shelf. Gravity core DA17-NG-ST03-039G is presented here. The core is located in the area of the North East Water Polynya (NEW Polynya), a seasonally-open water area with great importance to marine ecosystems (Barber and Massom, 2007; Schneider and Budéus, 1994) (Fig. 1b and Fig. 2). The key location of this core allows the investigation of Early to Mid Holocene changes in environment, including the ocean dynamics and sea-ice configuration of the western Fram Strait, as the core site area is submerged by both cold Polar Waters from the Arctic Ocean and warmer, saline Atlantic Waters derived from the North Atlantic Current system.

We thus aim to evaluate the interaction between changes in ocean currents, especially influx of Atlantic subsurface water, sea-ice conditions and the Northeast Greenland Ice Stream (NEGIS) dynamics from the late deglacial phase until the end of the Holocene Thermal Maximum. We base our study on a multiproxy investigation, encompassing benthic foraminiferal assemblages, core scanner X-ray Fluorescence and magnetic susceptibility measurements, colour scans, radiographic images and grain size analyses of marine sediment core DA17-NG-ST03-039G. This enables us to reconstruct the past variability in Atlantic and Polar Water advection to the northern section of the Northeast Greenland shelf and constrain the past ice sheet extent and deglacial conditions in the study area.

2. Regional settings

2.1. Modern oceanography

The Fram Strait is 500 km wide and represents a major gateway of deep-water exchange between the North Atlantic and Arctic Ocean (Klenke and Schenke, 2002). Southward outflow from the Arctic Ocean via the Fram Strait to the Nordic Seas and subsequently the North Atlantic Ocean is conveyed by the EGC ($T < 0$ °C, $S < 34.5$; Aagaard and Coachman, 1968), transporting drift ice and freshwater towards lower latitudes along the Northeast Greenland shelf (Haine et al., 2015). The atmospherically-driven Transpolar Drift circulation system in the Arctic Ocean feeds the EGC and thus controls its freshwater and sea ice variability (Deser et al., 2000; Dyke et al., 1997).

From the south, relatively warmer Atlantic Water masses are transported to higher latitudes via the West Spitsbergen Current (WSC) ($T > 2$ °C, $S > 35$; Hopkins, 1991), emanating from the Norwegian Atlantic Current (NAC) (Aagaard and Coachman, 1968a; Schaffer et al., 2017). In the Fram Strait, about half of the Atlantic-derived WSC is deflected westward across the strait between 76 and 81°N and transformed into the intermediate Return Atlantic Current (RAC) (T ~0–2 °C, S ~34.9–35; Hopkins, 1991) (Aagaard and Coachman, 1968b; Hattermann et al., 2016; Marnela et al., 2013). The RAC flows southward transporting Return Atlantic Water (RAW) along the Northeast Greenland shelf, where it mixes with the cold Polar component of the EGC (Bourke et al., 1987; de Steur et al., 2014). This increases its density and eventually leads to the formation of the dense overflow water in Denmark Strait linked to the AMOC (Hansen and Østerhus, 2000; Harden et al., 2016; Håvik et al., 2017; Strass et al., 1993). Another component of the WSC continues northward into the Arctic Ocean, where it cools and freshens, while flowing cyclonically in the Eurasian and Canadian basins at intermediate water depths (Rudels et al., 1994), eventually returning to the Fram Strait where it joins the RAW at 78°N; it is referred to as Arctic Atlantic Water (AAW) (T ~0.8–2 °C, S ~34.8; (Locarnini et al., 2019; Richter et al., 2018; Schaffer et al., 2017). Both these Atlantic-derived water masses contribute to the lower section of the EGC (Håvik et al., 2017; Rudels et al., 2012).

Melting of the three outlet glaciers of the NEGIS contribute to the upper fresh-water layer on the Northeast Greenland continental shelf in the western part of the Fram Strait. In the proximity of our core site, two major glaciers, Nioghalvfjerdsfjorden Glacier (79G) and Zachariæ Isstrøm glacier (ZI), terminate into the sea; together they account for the majority of the NEGIS drainage (>15% of the GIS drainage) (Rignot and Kanagaratnam, 2006). Recent studies suggest there is a link between intensified anticyclonic surface and subsurface inflow of warmer Atlantic Water via the Norske Trough (Fig. 1b) to the NEGIS front, causing ice retreat events of the 79G and ZI (Mouginot et al., 2015; Schaffer et al., 2017; Topp and Johnson, 1997). In addition, the Westwind Trough, might allow supplementary inflow of Atlantic Water across the shelf towards the marine-terminating outlet glaciers (Arndt et al., 2015, 2017; Schaffer et al., 2017). The source of subsurface Atlantic Water in Norske Trough is dominated by the comparatively warm and saline RAW, whereas Westwind Trough (Fig. 1b) is mostly influenced by the colder AAW transported by eddy flows from the EGC (Rudels et al., 2012; Schaffer et al., 2017). A 250 m deep sill located between the two trough systems causes this separation of the two Atlantic derived subsurface water masses (Budéus et al., 1997). However, the RAW that enters Norske Trough causes melting of the 79G and ZI (Yang et al., 2020), decreasing the density of Atlantic Water. This potentially allows a through flow of these modified Atlantic Waters across the sill and into Westwind Trough (Schaffer et al., 2017).

2.2. Geology of the hinterland

The 79G is flanked by Proterozoic sediments comprised by sand and siltstones cut by Mesoproterozoic dolorites. Few outcrops of finely crystalline Ordovician dolomites can be observed further upstream SE to the 79G. Additional carbonate-bearing outcrops are located inland NW to the 79G. Paleoproterozoic crystalline basement rocks (orthogneiss) dominate further downstream the 79G along the coastline (Higgins, 2015).

2.3. Sea ice and polynya

Approximately 10% of the Arctic sea-ice area is transported through the Fram Strait via the EGC each year (Kwok, 2009; Smedsrud et al., 2017). Consequently, the northwestern part of the Fram Strait is affected by heavier sea-ice conditions. In contrast,

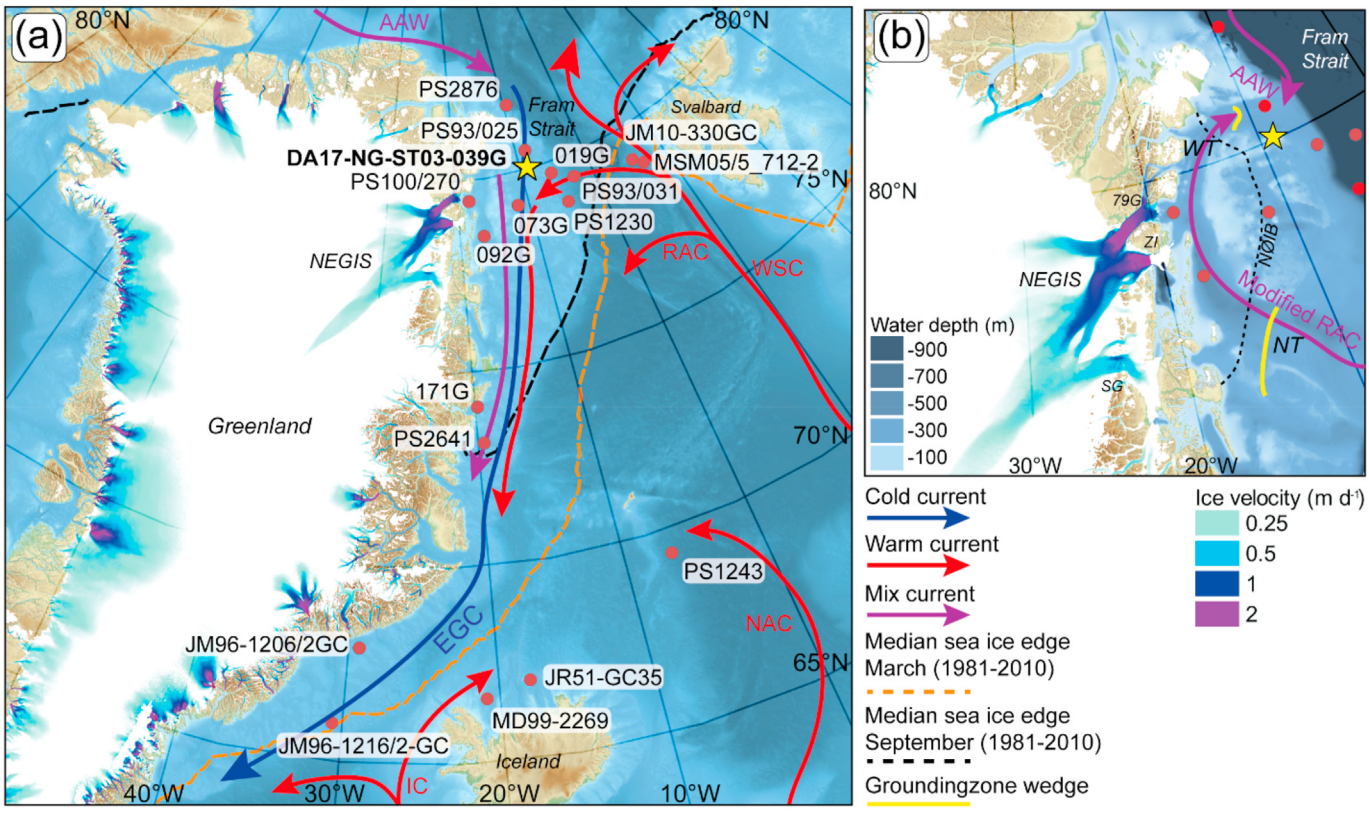

Fig. 1. Inset maps of the study site including main ocean currents, sea-ice extent (NSIDC, 2020) and locations of marine sediment cores mentioned in the text. (a) The studied core is marked by a yellow star. PS2876 (Nørgaard-Pedersen et al., 2008), PS93/025 (Syring et al., 2020b; Zehnich et al., 2020), PS100/270 (Syring et al., 2020a), JM10-330 GC (Consolaro et al., 2018), MSM05/5_712−5 (Werner et al., 2013), 019G (Rasmussen et al., 2022), PS93/031 (Spielhagen and Mackensen, 2021), 073G (Pados-Dibattista et al., 2022), 092G (Davies et al., 2022), PS1230 (Bauch et al., 2001), 171G (Jackson et al., 2022), PS2641 (Müller et al., 2012; Perner et al., 2015a), PS1243 (Bauch et al., 2001), JM96-1216/2 GC (Jennings et al., 2006), JM96-1206/2 GC (Perner et al., 2016), JR51-GC35 (Cabedo-Sanz et al., 2016), MD99-2269 (Cabedo-Sanz et al., 2016; Harning et al., 2021). (b) Close-up on core DA17-NG-ST03-039G (yellow star), local bathymetry and topography, ice stream velocity and the three major outlet glaciers of the Northeast Greenland Ice Stream, NG: Nioghalvfjerdsfjorden Glacier, ZI: Zachariæ Isstrøm glacier, SG: Storstrømmen Glacier. The positions of grounding zone wedges are derived from Arndt et al. (2017). Other abbreviations: WT: Westwind Trough, NT: Norske Trough, NØIB: Norske Øer Ice Barrier. The bed topography and ocean bathymetry data are derived from GEBCO (Weatherall et al., 2015) and BedMachine v3 (Morlighem et al., 2017), and the ice stream velocity data are derived from Sentinel- SAR data gathered from December 28, 2017 to February 28, 2018 (Nagler et al., 2015).

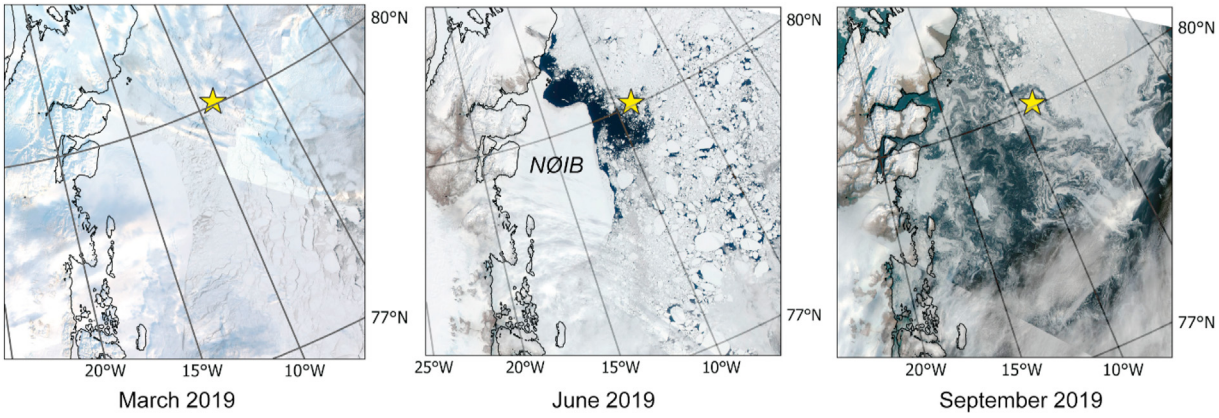

Fig. 2. Local seasonal sea-ice conditions for 2019 derived by MODIS satellite data (NASA, 2018). The core site for DA17-NG-ST03-039G is marked by the yellow star. NØIB: Norske Øer Ice Barrier.

sea-ice extent along the eastern side varies seasonally; it depends on the strength and temperature of the Atlantic Water inflow and strength of the EGC. In fact, the air-sea surface heat balance is positive in the western Fram Strait during summers, meaning that the sea surface is gaining heat. Hence if the EGC did not transport drift ice in the western Fram Strait, the area would be ice-free in summer (Schneider and Budéus, 1994). The influence of warm Atlantic Water advection in the eastern Fram Strait makes West Spitsbergen the northern-most ice-free marine environment during the winter season (Aagaard, 1982; Vinje, 1977). Occasionally,

ice-free areas occur on the Northeast Greenland shelf related to the seasonal coastal NEW Polynya (Koch, 1945; Vinje, 1970). The NEW Polynya occupies an area of up to 44,000 km^2 on the Northeast Greenland shelf at around 79 °N (Fig. 2) (Schneider and Budéus, 1994; Wadhams, 1981). The polynya formation depends on the landfast ice of the Norske Øer Ice Barrier (NØIB) at 79 °N (Figs. 1b and 2). The NØIB acts as a barrier for ice floes transported by a northward coastal-bound current, together with the strength of offshore winds pushing sea ice away from the area (Schneider and Budéus, 1994). The NEW polynya starts forming in April/May and is fully established in summers; it is dominated by positive air-sea surface heat balance and strong offshore winds (Schneider and Budéus, 1994). In winter, the area is partially sea-ice covered, however, the present sea ice is less dense compared to the surrounding sea ice located further offshore (Schneider and Budéus, 1994; Smith et al., 1990). The seasonal open water area is of great importance for marine ecosystems that benefit from the melting of the sea-ice edge, releasing nutrients to the water masses promoting marine productivity (Barber and Massom, 2007; Schneider and Budéus, 1994). The maintenance and formation of the coastal NEW Polynya is still not fully understood. Yet, a recent study suggests that the seasonal NEW Polynya conditions were fully developed at 1 cal ka BP, related to the establishment of stable sea-ice edge conditions (Syring et al., 2020b).

3. Material and methods

3.1. Conductivity-temperature-depth profile

A conductivity-temperature-depth profile (CTD; DA17-NG-ST03-023CTD; 80.044°N/8.955 °W, 389 m water depth) was measured along a vertical depth profile using a SEABIRD 911 system of RV *Dana*, to identify the different water masses. Here we show the temperature and practical salinity profiles for the study site (Fig. 3).

3.2. Sediment core retrieval

During the NorthGreen2017 cruise on board the research vessel *Dana* (Seidenkrantz et al., 2018), we collected the gravity core DA17-NG-ST03-039G at the edge of the Westwind Trough on the outer Northeast Greenland shelf (80.037 °N/8.923 °W, 390 m water depth) (Fig. 1). The location was selected based on a site survey using a shallow seismic survey (*Innomar SES-2000 Deep, Narrow-Beam Parametric Sub-Bottom Profiler*), which showed the presence of soft and likely undisturbed sediments.

After retrieval, gravity core DA17-NG-ST03-039G was divided into four sections on board and kept in cold storage at ca. 3 °C; it was subsequently split lengthwise in the laboratory at the Department of Geoscience, Aarhus University.

3.3. Lithology and grain size

The colour of the marine sediment gravity core was described using a Munsell colour chart. Grain size measurements were conducted for every 4 cm of the gravity core (1 cm wide samples), except for the bottom interval; 301–317 cm, where every centimetre was sampled. All samples were measured with a Sympatec HELOS laser (He–Ne type) diffractometer equipped with a R4 lens capable of measuring particles in the size range of 1.8–350 μm at the Department of Geoscience, Aarhus University. The average of 3–5 measurements for each sample depth was calculated. Moreover, the grain size results were grouped into a clay fraction (<2 μm), silt fraction (2–63 μm) and sand fraction (63–200 μm) using the sediment grain size statistical package GRADISTAT (Blott and Pye, 2001). The dry weight of size fraction >1 mm from the wet sieving of foraminifera samples was used to calculate the ice rafted debris (IRD) content (mg pr. g wet sediment).

3.4. Radiocarbon dating and age model

An age-depth model for DA17-NG-ST03-039G was established based on 13 AMS (Accelerator Mass Spectrometer) radiocarbon dates performed separately on either mixed benthic (representing the general assemblage at the sample level, in particular *Cassidulina neoteretis, Cassidulina reniforme, Islandiella norcrossi, Elphidium clavatum* and *Nonionellina labradorica*) or planktonic (primarily *Neogloboquadrina pachyderma*) foraminiferal species, measured at the Eidgenössische Technische Hochschule (ETH) Laboratory, Ion Beam Physics, in Zürich (Table 1). The radiocarbon analyses were performed on a compact AMS system equipped with a gas ion source directly on the CO_2 from 200 to 2000 μg from dissolved biogenic carbonate (Wacker et al., 2013). If possible (>300 μg carbonate), a leach fraction was also measured for quality control (Bard et al., 2015). For sample depths 307.5, 310.5, 313.5, and 316.5 cm paired radiocarbon dating of mixed benthic and mixed planktonic

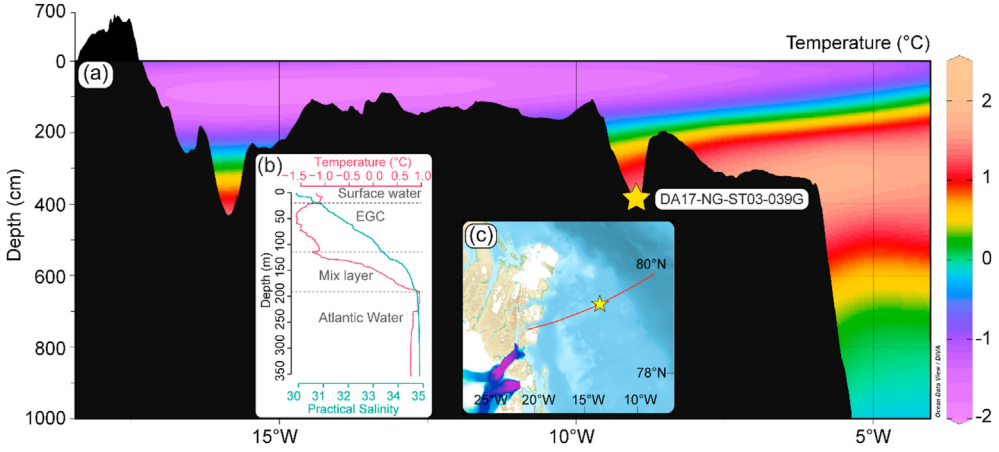

Fig. 3. (a) West-east transect at ~80°N (across the core site; yellow star) showing the annual average temperature distribution of the water masses at the study site derived from the World Ocean Atlas (Locarnini et al., 2019). Panel (b) shows the results of the CTD profile (DA17-NG-ST03-023CTD), where the different water masses mentioned in the text are marked. The red line in panel (c) shows the location of the transect.

Table 1
Overview of the radiocarbon datings of core DA17-NG-ST03-039G. Modelled median calibrated ages from sample depths marked with * are used in the age depth model. + Samples were small (<300 μg) and thus not leached.

Sample depth midpoint (cm)	Lab. ID	Material	^{14}C age (yr. BP)	Unmodelled calibrated age range (cal yr. BP), 2σ	Modelled median age (cal. yr. BP)
11	ETH-106021	Mixed benthic foraminifera	2830 ± 80	2159–2673	n.a.
37.5	ETH-106022	Mixed benthic foraminifera	2775 ± 70	2101–2601	n.a.
52.5	ETH-107365	Mixed benthic foraminifera	2220 ± 60	1439–1838	n.a.
83*	ETH-106023+	Mixed benthic foraminifera	4210 ± 80	3857–4380	3920
112.5*	ETH-106024+	Mixed benthic foraminifera	4390 ± 100	4040–4677	4523
137.5*	ETH-106025+	Mixed benthic foraminifera	5090 ± 130	4876–5552	5253
167.5*	ETH-107366	Mixed benthic foraminifera	6000 ± 70	6000–6421	6160
192.5*	ETH-107367	Mixed benthic foraminifera	6355 ± 60	6396–6805	6697
197	AAR-29380	Unidentified shell fragment	5825 ± 29	5892–6198	n.a.
212.5*	ETH-107368	Mixed benthic foraminifera	7050 ± 70	7173–7537	7391
237.5*	ETH-106026	Mixed benthic foraminifera	8385 ± 70	8524–8994	8659
272.5*	ETH-106027	Mixed benthic foraminifera	9200 ± 70	9529–10065	9772
292.5*	ETH-106028	Mixed benthic foraminifera	9635 ± 70	10151–10587	10413
307.5	ETH-107369	Mixed benthic foraminifera	10120 ± 70	10765–11243	n.a.
307.5*	ETH-107370	Mixed planktonic foraminifera	10055 ± 80	10680–11195	11039
310.5	ETH-115691	Mixed benthic foraminifera	10480 ± 70	11256–11807	n.a.
310.5*	ETH-115692	Mixed planktonic foraminifera	10190 ± 60	10880–11340	11188
313.5	ETH-115693	Mixed benthic foraminifera	11080 ± 90	12121–12677	n.a.
313.5*	ETH-115694	Mixed planktonic foraminifera	11080 ± 90	12121–12677	12435
316.5	ETH-106029	Mixed benthic foraminifera	12255 ± 80	13358–13842	n.a.
316.5*	ETH-106030	Mixed planktonic foraminifera	12070 ± 60	13202–13584	13291

foraminiferal species were measured. For these sample depths, only the radiocarbon dates based on mixed planktonic species were used in the age depth model. All radiocarbon ages were calibrated with the OxCal v4.4.4 software (Ramsey, 2008; Ramsey and Lee, 2013) using the Marine20 calibration curve (Heaton et al., 2020). For the calibration we applied a constant marine reservoir correction of $\Delta R = 0$ years compared to Marine20 (Heaton et al., 2020; Reimer and Reimer, 2001). According to Heaton et al. (2020) the newest marine calibration curve Marine20 should not be applied in Arctic research, since sea-ice cover impacts the local reservoir ages. However, uncertainties regarding the effect of sea-ice cover on the reservoir ages are also applicable for the Marine13 calibration curve (Reimer et al., 2013), which numerous studies conducted on Arctic marine sediments use (e.g. Perner et al., 2016; Syring et al., 2020a; Van Nieuwenhove et al., 2020). Thus, the Marine20 calibration curve has been applied for radiocarbon calibration in many studies performed on marine sediments from the Polar regions (Davies et al., 2022; El bani Altuna et al., 2021; Farmer et al., 2021; Pados-Dibattista et al., 2022). A depositional *P_sequence* model was used for the age-depth modelling with a k value of 0.5 (Ramsey, 2008; Ramsey and Lee, 2013).

3.5. Foraminifera

Approximately 1-cm wide slices were subsampled for foraminiferal analysis at every 5 cm of the gravity core from 83 to 308 cm; every 1 cm of the bottommost 308–317 cm were subsampled. The wet sediment samples were weighed and wet sieved using three sieves with mesh sizes of 0.063, 0.100 and 1 mm. The separate fractions were dried in filter paper in an oven at 40 °C until dry. The dry filter papers were weighed before and after the sample material was put in glass vials. The 0.063 and 0.100 mm fractions were combined and used for benthic foraminiferal assemblage analysis, where both agglutinated and calcareous benthic species were identified and counted together in order to reach a total count of 300 specimens for all samples. The percentages of the various agglutinated and calcareous species were calculated based on the total benthic (agglutinated and calcareous) assemblage to obtain statistically reliable data. Fluxes of the calcareous benthic, agglutinated benthic and planktonic individuals were calculated based on individual species pr. gram sediment (ind./g) wet sediment weight (g), sedimentation rate (cm/ka) and density (g/cm^3) $\left(\text{Flux} = \frac{\text{ind.}}{\text{g}} \frac{\text{g}}{\text{cm}^3} \frac{\text{cm}}{\text{ka}}\right)$. We used a density of 1.6 g/cm^3 based on CT scan results of another marine sediment core close to Zachariæ Isstrøm, core DA17-NG-ST08-092G (78.501°N, 17.279°W, water depth: 583 m) (Davies et al., 2022). Stratigraphically-constrained hierachal cluster analysis was performed on the most abundant benthic foraminifera (>% 4 frequency in at least one sample depth) using an algorithm that operates on a dissimilarity matrix of squared Euclidean distances in the Rioja software (Grimm, 1987; Juggins, 2020). The "broken-stick" method was used for the identification of zones (Bennett, 1996; Juggins, 2020).

3.6. Core scan and X-ray fluorescence

The X-ray fluorescence core scanning method utilizes X-rays to scan and log the bulk geochemical elemental composition of a sediment core with minimal destruction and disturbance of the sediment surface (Croudace et al., 2006, 2019; Rothwell and Croudace, 2015). The gravity core was scanned at the Department of Geoscience, Aarhus University, using an ITRAX core scanner equipped with a Molybdenum X-ray tube with generator settings 30 kV, 30 mA and exposure time 10 s to log the elemental spectra from aluminium to uranium at a 0.2 mm resolution. The bottom 2 cm of the core was not scanned due to a mistake in the laboratory. A running average with window length 0.3 cm was calculated for all shown elements and element ratios to eliminate noise. In addition, the magnetic susceptibility (volume) of the core was measured for every 5 cm using a Bartington magnetic susceptibility system, with a MS2E high-resolution point-sensor and a MS2I Sensor.

High-resolution line scan and radiographic images (voltage: 60 kV; current: 45 mA; exposure time: 2000 ms) were made with the ITRAX core scanner: The radiographic measurement is quantified as RAD (X-ray intensity), and the colour image is quantified as RGB values, averaged to grayscale values.

4. Results

4.1. CTD and water mass distribution

The present surface water (0–20 m) at the Northeast Greenland shelf at ~80°N is characterized by temperatures and salinities of about −1.2 °C and 30–31 in September, based on CTD measurements collected at the core site in September 2017 (Fig. 3b). This surface layer comprises Polar Water mixed with glacial and seaice meltwater. At 20–110 m water depth a cold-water mass with temperatures of −1.5 °C to −1.2 °C and increasing salinities (31–33.5) is assigned to the Polar Water component of the EGC. The warmer water mass that underlies the Polar Water is characterized by increasing temperatures in the range of −1.3 °C to −1 °C and salinities 33.5 to 34.9 between 110 m and 190 m, which could be a result of mixing of the AAW and the Polar Water component of the EGC. Below ~190 m water depth the warmest water mass is observed with temperatures 0.7 °C–1 °C and salinity ~34.9, which is ascribed to AAW with potential minor contributions from RAW (Schaffer et al., 2017), here just designated "Atlantic Water". According to the World Ocean Atlas annual average temperature measurements, the Atlantic Water exceeds 2 °C at ~80°N (Fig. 3) (Locarnini et al., 2019).

4.2. Age model

The results of the age-depth model of core DA17-NG-ST03-039G are shown in Fig. 4 and Table 1. The AMS ^{14}C date performed on shell fragments (197 cm core depth) is considered an outlier and was omitted from the age model. Moreover, due to the ambiguity of the top three radiocarbon dates (11.0, 37.5, and 52.5 cm), possibly representing an interval with reworked sediments; this section of the core was excluded from further analyses and interpretation in the present study. Consequently, we will focus on the depth interval 83–317 cm, where 13 ^{14}C dates measured on foraminifera show a general good agreement without reversals, corresponding to the period between 13.3 and 3.9 cal ka BP. For the sample depths, where both planktonic and benthic foraminifera were dated (307.5, 310.5, 313.5, and 316.5 cm), the offset ranged between 0 and 290 years with the planktonic material returning the younger ages but otherwise no distinguishable pattern (Table 1). After calibration however, the calibrated 2-sigma age ranges show overlap between the benthic and planktonic results (Table 1), despite the use of the same constant reservoir age correction. In the final age model, we rely on the benthic dates for the intervals where no planktonic material was available (Fig. 4). Since there was no trend in benthic-planktonic offset, no further reservoir correction or uncertainty was applied to the benthic samples. This could result in an overestimation of the modelled age for the upper part of the core, although this is likely to be very minimal considering the relatively shallow water depth of the site and the presence of well-ventilated Atlantic Water.

4.3. Sediment properties

The recovered sediment mainly consists of brown clayey silt (Fig. 4). The lowermost 20 cm (317-297 cm) is characterized by several smaller pebbles and a slight increase in the visible grain size distribution. Additionally a large drop stone of 4 cm was found at core depth 272 cm (9.8 cal ka BP). The core showed black spots throughout most of the core. The grayscale values show high values at the bottom of the core indicative of light-coloured sediment, hereafter the values remain relatively stable, until 120 cm core depth where the increase towards the top indicate gradually lighter coloured sediments. The results of the RAD show low values at the bottom of the core related to high density of the sediments. Hereafter, the RAD is stable until one high peak centred at 185 cm core depth implying low sediment density. After this, the RAD values decrease slightly reporting high sediment densities until 20 cm core depth where values increase towards the top of the core indicating decreasing density. The small peak observed at 117 cm core depth is located at a section shift.

Four zones were defined based on the stratigraphically-constrained hierarchal cluster analysis of the benthic foraminiferal dataset. The grain size distribution does not vary vastly throughout the core; however, the sand fraction is more dominant in the beginning of zone I (c. 13.3 to 11.7 cal ka BP) concurrent to high IRD, Ca/Sr, Ca/Fe and magnetic susceptibility (Fig. 5). The magnetic susceptibility reaches peak values at c. 12.3 cal ka BP, whereafter values decrease, and remain stable in the end of zone I. The IRD shows a large peak at 11.0 cal ka BP. After c. 11.1 cal ka BP (end of zone I), most of the grainsize and XRF data do not show great variability. However, Ca/Fe and Ca/Sr ratios decrease and remain relatively low and stable for the rest of the core except for one peak at c. 6.9 cal ka BP in zone III. Magnetic susceptibility is generally fluctuating in zone II and III, peaking at c. 10.5 cal ka BP and c. 6.5 cal ka BP, followed by lower less fluctuating values in zone IV. The sedimentation rate is relatively very low in zone I (~4.2 cm/ka) and it increases gradually and stepwise throughout zones II-IV with relatively higher sedimentation rates at c. 11.1, 9.8, 6.7, and 4.5 cal ka BP.

4.4. Foraminiferal fauna of core DA17-NG-ST03-039G

The benthic foraminiferal assemblages are presented as percentages (Fig. 6), based on the combined agglutinated and calcareous species counts, since in some depth intervals the calcareous benthic species were scarce. In total, 72 different benthic species were identified (45 calcareous and 27 agglutinated). The planktonic foraminiferal counts were in general low (0–294 ind./g wet sed.), whereas the combined benthic species were more abundant (19–1456 ind./g wet sediment). Both benthic and calcareous species showed minor signs or no signs of post-mortem dissolution and were thus generally well preserved throughout the core.

4.4.1. Zone I: 13.3–11.1 cal ka BP

This zone contains the highest absolute concentrations of both benthic and planktonic foraminifera, reaching peak values of 1456 and 294 individuals/g sediment at c. 11.2 cal ka BP, respectively. At 13.3 cal ka BP, the benthic assemblage is dominated by high abundances of *Cassidulina neoteretis* (37%) and *Stetsonia horvathi* (25%), however, these species drop at c. 12.4 cal ka BP, where *Epistominella arctica* reaches its highest value of ~67% in the entire record. Additionally, *Islandiella norcrossi* shows highest abundances for the core in this zone, reaching ~11% at 13.0 cal ka BP. In contrast, the abundances of *Elphidium clavatum* (~2.5% on average) and *Elphidium albiumbilicatum* (~0.6% on average) are relatively low, whereas *Cassidulina reniforme* is moderately high (~9.2% on average). The agglutinated species are nearly absent.

4.4.2. Zone II: 11.1–9.4 cal ka BP

This zone is characterized by abruptly decreasing and fluctuating calcareous benthic and planktonic fluxes. The benthic species are 40 times more abundant than the planktonic species on average. Amongst the most abundant calcareous species are *C. reniforme* (~11% on average), *C. neoteretis* (~18% on average) and *E. clavatum* (~32% on average).

The abundance of *S. horvathi* increases in the beginning of this zone (~6%), where it intermittently disappears at c. 10.3–9.9 cal ka BP coinciding with highest abundance of *E. clavatum* (~60%). This is

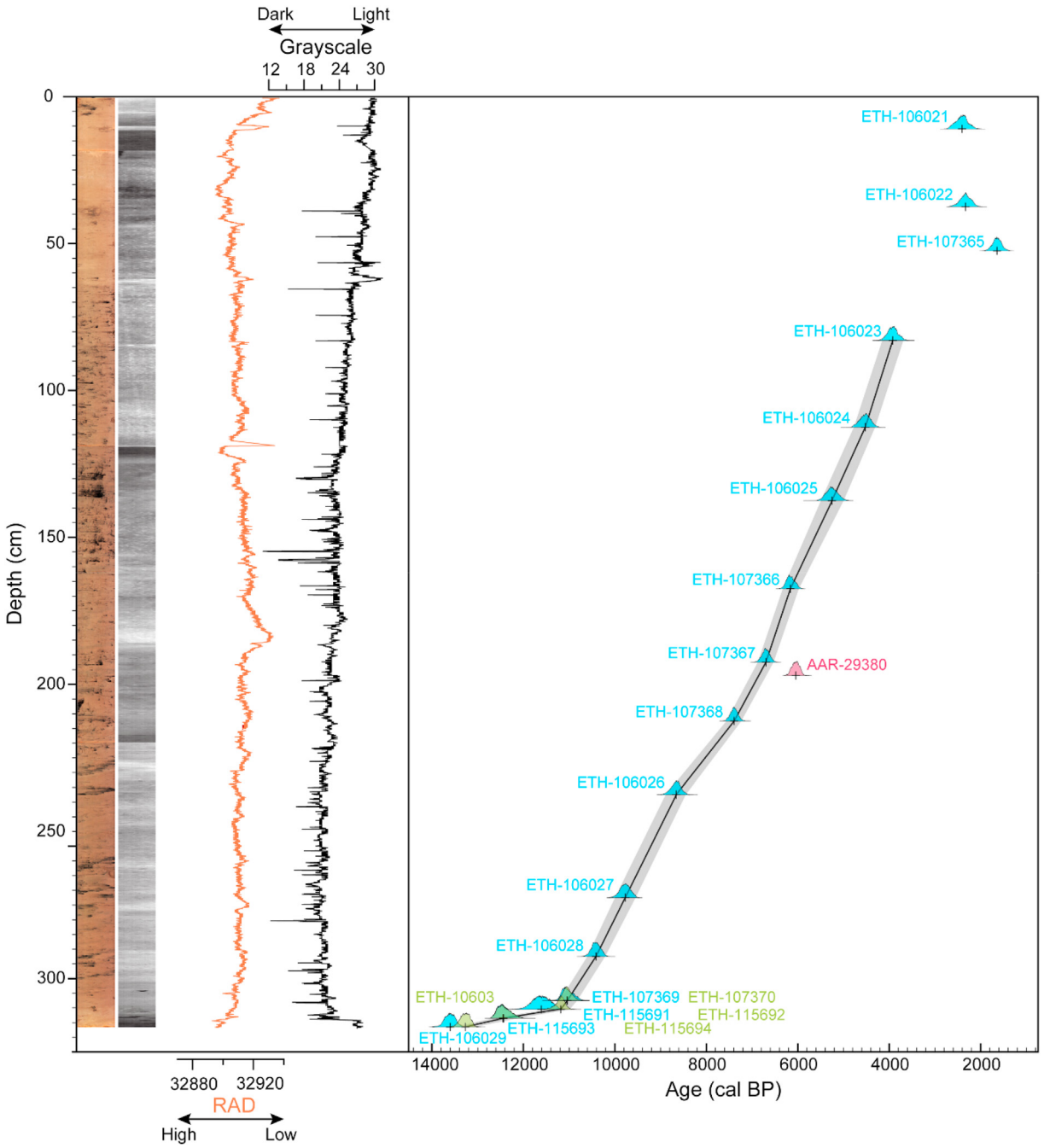

Fig. 4. Core images and chronology of sediment core DA17-NG-ST03-039G. The left panel shows high-resolution core scan images with increased brightness and contrast, radiograph images, related RAD intensity and grayscale values of the core. The right panel includes radiocarbon dates from core DA17-NG-ST03-039G, together with the benthic and planktonic foraminifera based age-depth model. Blue, green and red age distributions show calibrated radiocarbon ages based on mixed benthic foraminifera, mixed planktonic foraminifera and shell fragments, respectively. The grey envelope represents the modelled 2σ range. The solid black line indicates the median modelled ages.

followed by increasing percentages in both *S. horvathi* and *E. arctica* towards the end of this zone. The two calcareous species *Stainforthia feylingi* and *Nonionellina labradorica* both increase in abundance throughout this zone, whereas *Buliminella elegantissima* exhibit decreasing abundance by the end of this zone. *I. norcrossi* show much lower and fluctuating values compared to the preceding zone.

The agglutinated taxa are more abundant in this zone compared to zone I, where *Psammosphaera fusca* and *Portatrochammina bipolaris* are the most abundant. *P. bipolaris* constitute 42% of the total benthic foraminiferal assemblage at c. 10.6 cal ka BP.

4.4.3. Zone III: 9.4–6.2 cal ka BP

In this interval, the fluxes are relatively stable and vary in line with the changing sedimentation rates. The benthic foraminifera are still dominant. The most abundant calcareous species in this zone include *C. neoteretis*, *I. norcrossi*, *S. horvathi, E. arctica, N. labradorica, S. feylingi, B. elegantissima* and *C. reniforme*. *S. horvathi* is high from 9.3 to 8.2 cal ka BP, where after it drops to overall low values of about 2% in this zone. *E. clavatum* decreases after c. 9.4 cal ka BP and is generally stable in abundance throughout this zone (~15% on average). 7.9 cal ka BP records the highest abundance of the calcareous species *B. elegantissima* (~8%). At c. 7.0 cal ka BP

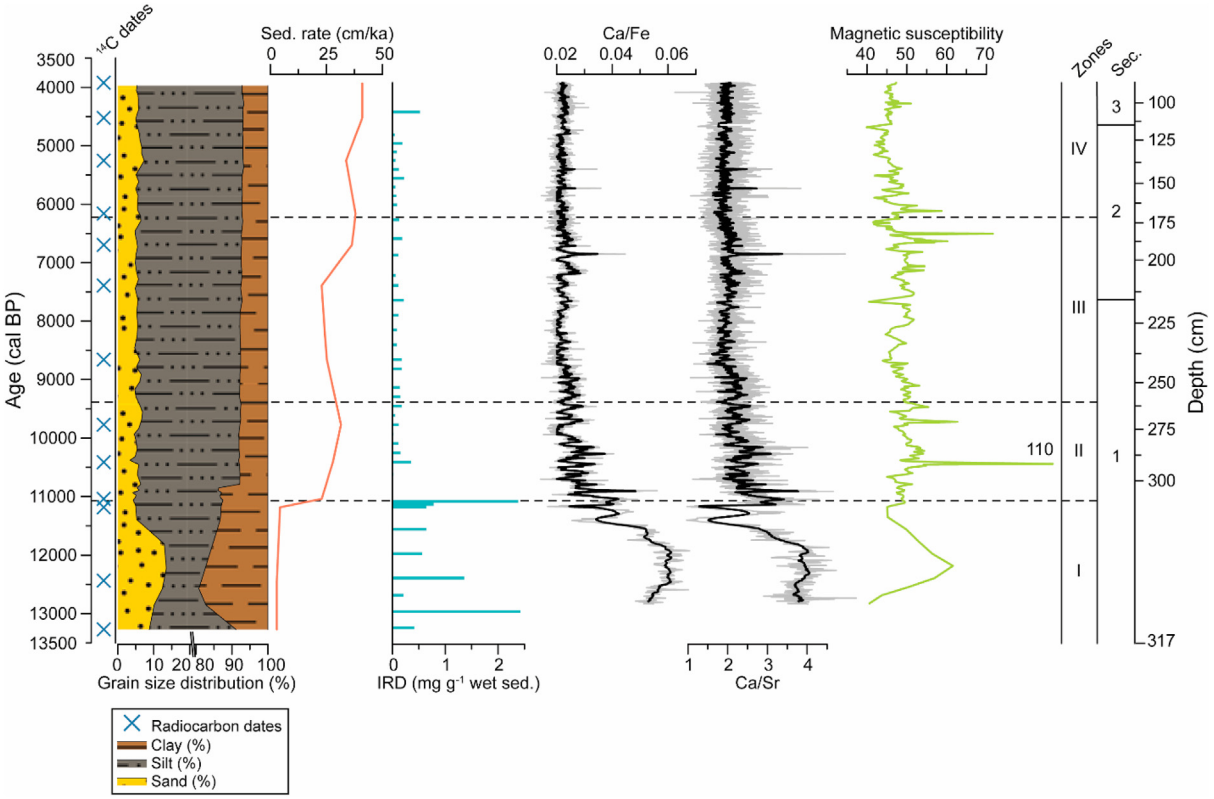

Fig. 5. Sediment properties of core DA17-NG-ST03-039G, including section divisions, grain size distribution, sedimentation rate, IRD, selected elements from the XRF core scan, where darker coloured lines show the running average with window length 0.3 mm and magnetic susceptibility. The benthic foraminiferal zones are indicated on the right side of the plot together with core section divisions. Depth intervals with radiocarbon dates are shown to the left.

I. norcrossi records its highest abundance of the zone (~7%), where *C. neoteretis* (~22%) and *C. reniforme* (~14%) also exhibit high percentage frequencies. All three species appear less abundant in the end of the zone. The abundances of *E. arctica, N. labradorica* and *S. feylingi* coexist as subsidiary species throughout the zone, with highest combined abundances centred at c. 6.4 cal ka BP of ~14%, followed by a decreasing trend in all three species.

The agglutinated species continue to increase gradually, with high occurrences of *Adercotryma glomerata, Earlandammina inconspicua, P. bipolaris* and *Recurvoides trochamminiformis*.

4.4.4. Zone IV: 6.2–3.9 cal ka BP

In this zone, the planktonic fluxes show the overall lowest values. Additionally, most of the calcareous species show low abundances reflected by the high agglutinated/calcareous ratio. Still, the calcareous species *E. clavatum, E. arctica, S. feylingi, C. reniforme,* and *E. albiumbilicatum* all show moderate relative frequencies. The agglutinated species *Spiroplectammina biformis* and *Textularia torquata* both exhibit high abundances for the first time. Additionally, *A. glomerata, P. bipolaris, P. fusca, E. inconspicua,* and *R. trochamminiformis* are similarly overall very abundant.

5. Paleoenvironmental interpretation

The reconstruction of the late glacial to Holocene bottom and subsurface water conditions on the Northeast Greenland shelf is based on the results and interpretations of the presented proxies: X-ray fluorescence spectroscopy, magnetic susceptibility, benthic foraminiferal assemblages and grain size distributions.

The bulk elemental ratio Ca/Fe allows differentiation between the relative contribution of biogenic marine and terrestrial Ca, and thus reflects local biogenic productivity, whereas relatively high Ca/Sr values may indicate input of detrital carbonate or lower occurrence of aragonite compared to calcite calcium carbonate (Figs. 5 and 7g) (Bahr et al., 2005; Croudace et al., 2006; Richter et al., 2006; Rothwell et al., 2006; Vare et al., 2009). However, one of the limitations of the XRF method is that changes in the sediments surface water content affect the intensity of especially the lighter elements, caused by radiation absorption of the water (Hennekam and de Lange, 2012). Changes in grain size and IRD distribution reveal variations in terrestrial influence, ice rafting and ocean current strengths and dynamics (Jennings et al., 2011; Stein et al., 1996). Variations in the magnetic susceptibility can reveal past changes in terrigenous input (Fig. 5), as high values can imply elevated input of magnetic minerals derived from bedrock (Kleiber and Niessen, 2000; Stein et al., 2004).

Foraminiferal species provide a basis for interpreting changes in the bottom and subsurface water environments. The agglutinated/calcareous benthic ratio can serve as an indicator of dissolution of calcareous tests and/or as a general indicator of unstable bottom and subsurface water conditions, which many of the calcareous species cannot tolerate (Aksu, 1983; Jennings and Helgadottir, 1994). However, the agglutinated tests tend to be more sensitive to compression and stress caused by the overlying sediments and thus a gradual downcore decrease in the quantity of agglutinated species might be caused by post-mortem breakage of tests due to increased pressure (Feyling-Hansen and Funder, 1990).

The benthic species *S. feylingi, N. labradorica,* and *E. arctica* are often linked to enhanced primary productivity potentially in relation to the proximity of a sea-ice edge or an oceanic front, releasing nutrients to the bottom waters (Jennings et al., 2004, 2020; Polyak et al., 2002; Rytter et al., 2002; Seidenkrantz, 2013; (Wollenburg

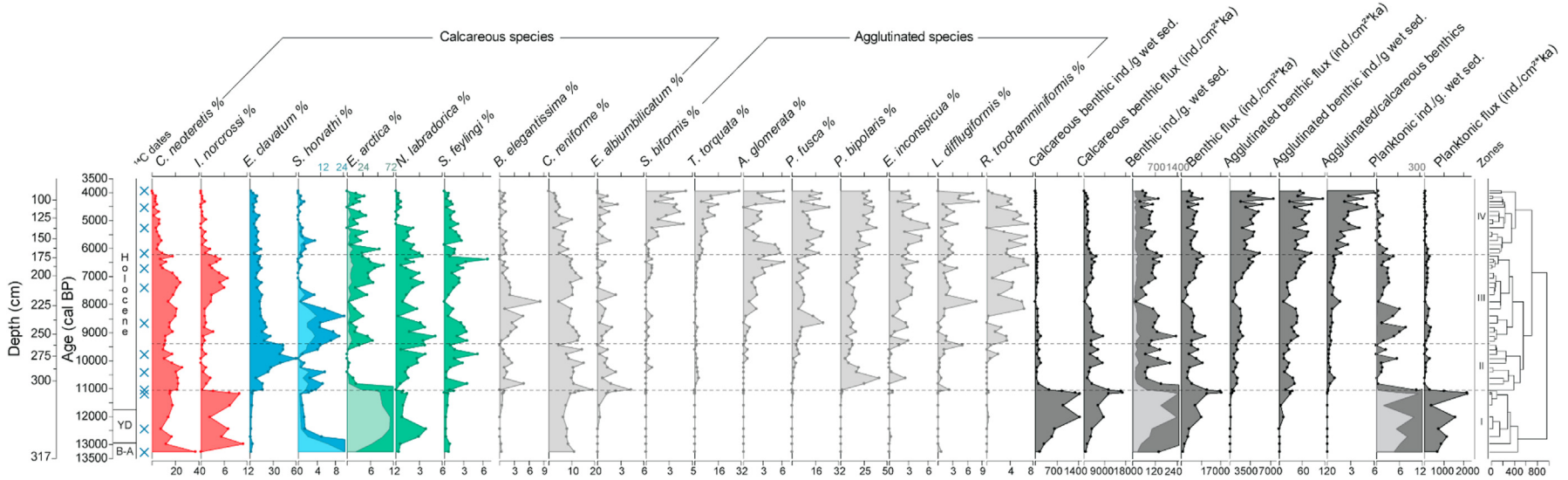

Fig. 6. Results of the foraminiferal assemblage analysis of DA17-NG-ST03-039G. All species with 4% frequency or higher in at least one sample depth of the total benthic foraminiferal assemblages are shown in the figure. The result of the stratigraphically constrained hierarchal cluster analysis is shown as a dendrogram to the far right. The division in zones is marked by dashed lines. Some calcareous species are colour shaded according to their known environmental preferences (see text for references), red: Atlantic Water, blue: fresh Polar Water and unstable conditions, green: high productivity. Blue crosses mark radiocarbon dates. Light colour shading for species *S. horvathi* and *E. arctica* as well as the number of benthic and planktonic individuals/g sediment indicate the full percentage distributions (top axis), whereas the dark shading shows a blow up of the same data; here the full percentage range of the data is not shown in some intervals. Foraminiferal zones are show to toward the right and main chronostratigrapical zones to the left (B-A = Bølling-Allerød, YD = Younger Dryas).

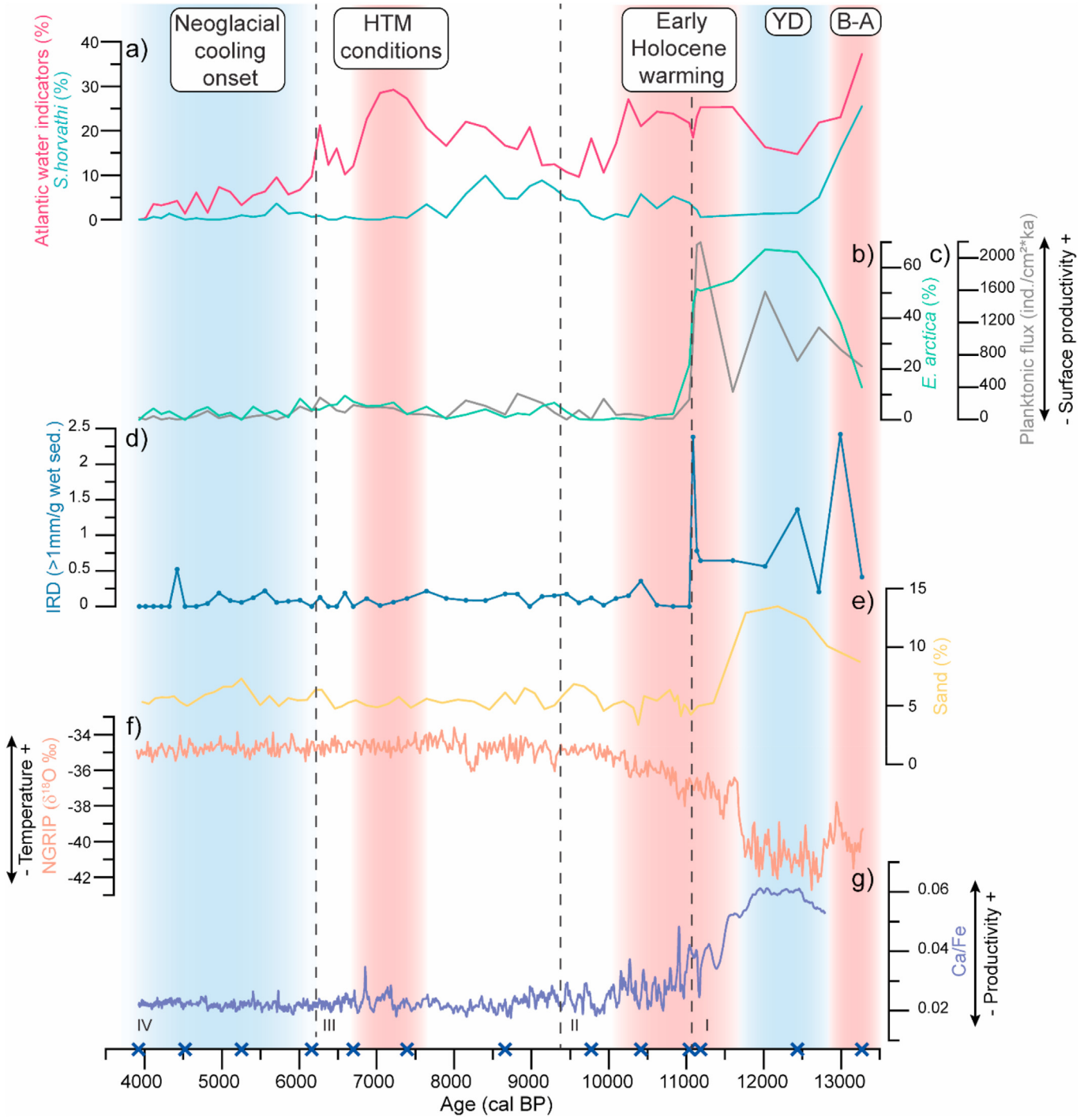

Fig. 7. Comparison between proxies from core DA17-NG-ST03-039G; a) Atlantic water indicator species and *S. horvathi*, b) *E. arctica*, c) planktonic flux, d) IRD, e) sand content, g) Ca/Fe, plotted together with $\delta^{18}O$ data from the NGRIP ice core (Rasmussen et al., 2006). Blue crosses mark radiocarbon dates. The blue bands mark cold periods, whereas the red bands indicate time intervals of increased Atlantic Water advection based on the abundance of the benthic Atlantic Water indicator species. Foraminiferal zones are marked by dashed lines (zone numbers are show at the bottom) and chronostratigraphical/climatic intervals are shown at the top (B-A = Bølling-Allerød, YD = Younger Dryas; HTM = Holocene Thermal Maximum).

and Mackensen, 1998)). *E. clavatum* is often found in areas affected by unstable conditions associated with turbid glacial meltwater flows (Hald et al., 1994) and its presence has previously been linked to relatively fresh and cold water masses facilitated by a strong EGC (Perner et al., 2012). However, *E. clavatum* does not seem to thrive under perennial sea-ice conditions (Jennings et al., 2020; Vilks, 1980). On the other hand, *S. horvathi* tolerates colder surface water conditions, since it has been found living beneath the

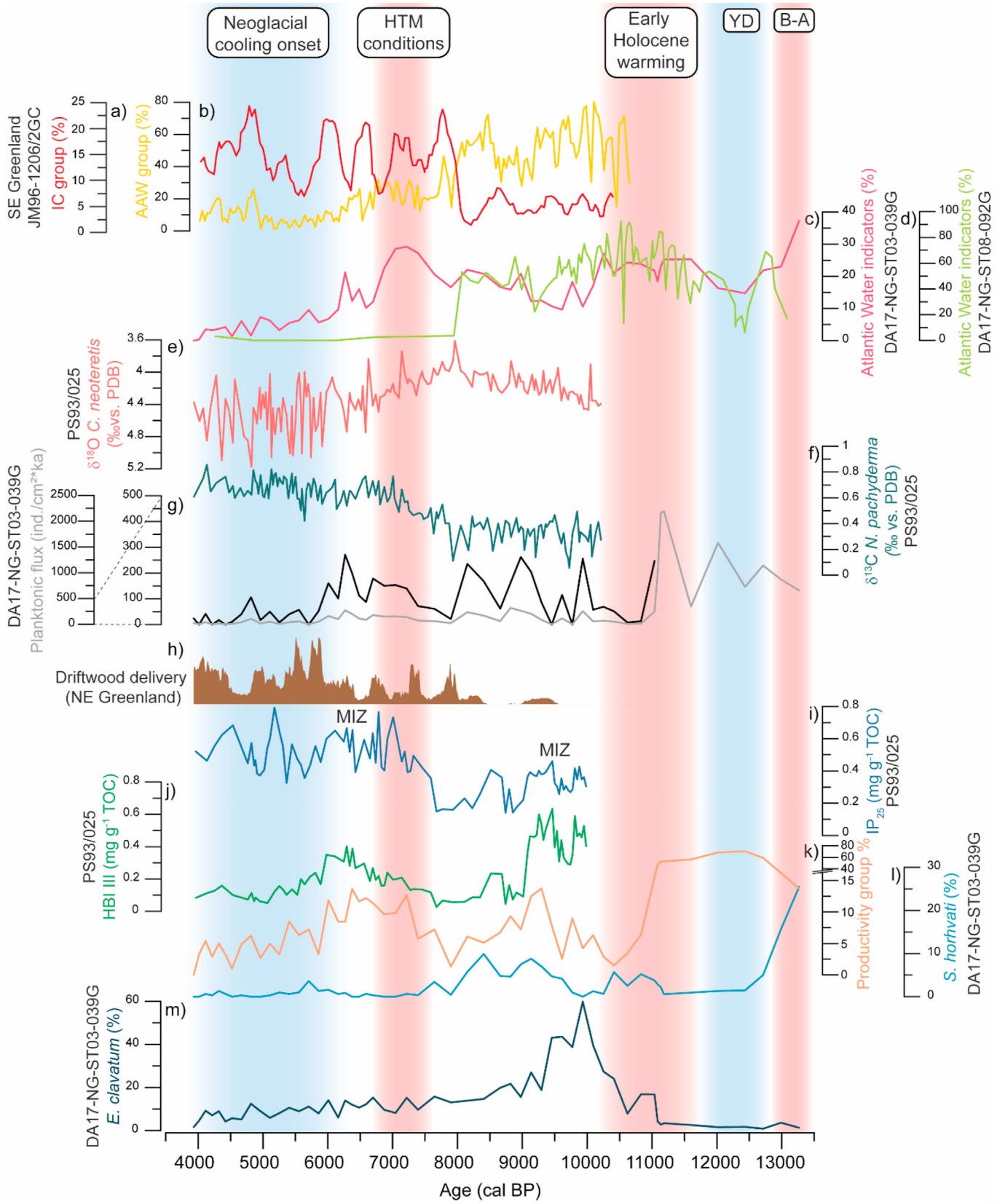

Fig. 8. Comparison between selected foraminiferal data from this study and proxy records from the Fram Strait and Southeast Greenland margin. a) IC group % (*C. neoteretis*) and b) AAW group % (*Melonis barleeanus* and *I. norcrossi*) from core JM96-1206/2 GC (Perner et al., 2016), c) Atlantic Water group % (*C. neoteretis* and *I. norcrossi*), d) Atlantic Water indicators % from core DA17-NG-ST08-092G (Davies et al., 2022), e) $\delta^{18}O$ *C. neoteretis* and f) $\delta^{13}C$ *N. pachyderma* from core PS93/025 (Zehnich et al., 2020), g) the planktonic flux, h) driftwood delivery record from Northeast Greenland (Funder et al., 2011b), i) IP_{25} and j) HBI III from core PS93/025 (Syring et al., 2020a), k) productivity group % (*S. feylingi, N. labradorica,* and *E. arctica*), l) *S. horvathi %,* m) *E. clavatum %.* MIZ: Marginal ice zone. Chronostratigraphical/climatic intervals are shown at the top (B-A = Bølling-Allerød,

Petermann Glacier ice tongue in northwest Greenland (Jennings et al., 2020). In addition, this species is commonly found in oligotrophic environments influenced by perennial sea-ice conditions in the shallower part of the Arctic Ocean (Husum et al., 2015; Wollenburg and Mackensen, 1998).

Given the location of our core site near the eastern mouth of the Westwind Trough and the NEW Polynya, our study area today receives Atlantic Water from the AAW, as implied in the CTD data (Fig. 3). Past inflow of RAW has been observed in the neighbouring core PS93/025 (Zehnich et al., 2020). Pervasive abundance of species *C. neoteretis* is often associated with influx of chilled Atlantic Water beneath a colder and fresher layer of Polar Water (Cage et al., 2021; Jennings and Helgadottir, 1994; Seidenkrantz, 1995). Furthermore, it's presence has been connected to both RAW and AAW masses (Wollenburg et al., 2004). In the northern Denmark Strait near the East Greenland coast, *I. norcrossi* has likewise been related to inflow of AAW (Cage et al., 2021; Perner et al., 2016).

5.1. Zone I, 13.3–11.1 cal ka BP

The highest sand and IRD content concurrent to low sedimentations rates (~4.2 cm/ka), high fluxes of planktonic and calcareous benthic foraminifera, low *E. clavatum* and high *C. neoteretis* abundances resemble the observations recorded in the outer Peterman Fjord from c. 7.0 cal ka BP, which was interpreted as distal glaciomarine conditions with Atlantic water influence (Jennings et al., 2022). Thus, we argue that overall similar distal glaciomarine conditions affected the outer Northeast Greenland shelf from 13.3 to 11.1 cal ka BP. Here, the elevated magnetic susceptibility values may be caused by the coarser grain size of magnetic minerals (Fig. 7d and e and Fig. 5). The high abundance of *S. horvathi* in the beginning of this zone (13.3 cal ka years BP) imply cold conditions presumably accompanied by heavy sea-ice concentrations (Figs. 7a and 8l). Concurrently, the relatively high abundance of *I. norcrossi* and *C. neoteretis* suggests a contemporary advection of Atlantic Water to the shelf underneath this extensive sea-ice cover.

E. arctica has been linked to mobile sea-ice productivity and seasonally ice-free areas (Jennings et al., 2020; Wollenburg and Mackensen, 1998). Thus, the large bloom in *E. arctica*, combined with high fluxes of both benthic calcareous and planktonic specimens and a drop in abundance of *S. horvathi* at ~12.9 cal ka BP (Fig. 7), suggest a change towards milder surface and subsurface water conditions with increased primary productivity in connection with more seasonal sea-ice. Furthermore, the similar depositional pattern observed in Ca/Sr and Ca/Fe ratios imply changes in the production of biogenic carbonate. Accordingly, increased local primary productivity is evident from c. 12.9 to 11.0 cal ka BP, inferred by relatively high Ca/Fe and Ca/Sr ratios (Figs. 5 and 8).

5.2. Zone II, 11.1–9.4 cal ka BP

A drop in Ca/Fe, Ca/Sr, IRD, sedimentation rate, sand fraction percentages, calcareous benthic and planktonic fluxes imply fewer ice rafting events and overall relatively lower productivity, also reflected by significantly lower *E. arctica* abundances (Figs. 5 and 7). High numbers of *C. neoteretis* in the beginning of this zone (c. 11.1 to 10.2 cal ka BP), point to advection of Atlantic derived water masses. The following drop in *C. neoteretis* after c. 10.2 cal ka BP coincide with increased frequencies in *E. clavatum* and stable *C. reniforme* abundances. This reflects glaciomarine conditions and/or a stronger advection of the sea ice and Polar Water loaded EGC (Hald et al., 1994; Perner et al., 2012). Further, the finding of a 4 cm large dropstone at ~272 cm (9.8 cal ka BP) likely relates to calving and/or meltwater release from the NEGIS. The sporadic occurrences of *N. labradorica* and *S. feylingi* might imply production of fresh phytodetritus related to a sea-ice environment with open water areas.

5.3. Zone III, 9.4–6.2 cal ka BP

In this interval, the foraminiferal fluxes vary in line with the changing sedimentation rates. The decreasing percentages of *E. clavatum* and slightly lower sedimentation rate from c. 9.4 cal ka BP are followed by very high abundances of *S. horvathi* together with relatively high numbers of the subsidiary species *E. arctica, N. labradorica,* and *S. feylingi* from 9.4 to 8.0 cal ka BP. This presumably reflect fresh phytodetritus production linked to the sea-ice margin (Figs. 5 and 6). The relatively low sedimentation rate around 8.6 cal ka BP might imply lower deposition of terrigenous material. Prolonged periods of ice cover can hinder sedimentation; this might be the cause of the low sedimentation rate observed here. At c. 8.0 cal ka BP, the low abundances of *S. horvathi, E. arctica, N. labradorica,* and *S. feylingi* point to reduced primary productivity, presumably caused by either an extension of the sea-ice cover or prolonged open water conditions. Contemporary elevated numbers of *C. neoteretis* might indicate gradually higher Atlantic Water incursion to the shelf.

The period c. 7.5 to 6.7 cal ka BP, centred at c. 7.1 cal ka BP, records the interval with highest influence of Atlantic-derived water, as suggested by high abundances of *C. neoteretis* and *I. norcrossi* in zone III (Fig. 6). Concurrently, at c. 7.1 cal ka BP there is an intermittent decrease in agglutinated species and increases in both the planktonic and calcareous benthic fluxes, pointing to a general amelioration of the subsurface and surface water conditions. The overall stable distribution of *C. reniforme* and relatively low *E. clavatum* in this zone relates to elevated and stable salinities potentially caused by a weaker EGC, since *C. reniforme* is more demanding of higher salinities compared to *E. clavatum* (Hald and Korsun, 1997). Notably, the Polar Water and perennial sea-ice indicator species *S. horvathi* does not seem to flourish under the relatively strong advection of Atlantic-sourced water masses. Following the peak in Atlantic Water indicator species at 7.1 cal ka BP, an increase in the high-productivity indicator species *E. arctica, N. labradorica,* and *S. feylingi* is observed, suggesting high primary productivity possibly linked to seasonal sea-ice conditions and passage of the sea-ice front. Noteworthy is the gradually increasing trend in the overall abundance of agglutinated specimens; this could be linked to better post-mortem preservation due to reduced sediment compression.

5.4. Zone IV, 6.2–3.9 cal ka BP

The overall increasing dominance of agglutinated species together with the lowest calcareous benthic flux values suggest generally cold bottom water conditions. Furthermore, the first noticeable appearance of the agglutinated species *T. torquata* and *S. biformis* record cold bottom water conditions (Fig. 6) (Lloyd, 2006; Perner et al., 2012; Vilks, 1969). This, together with the relatively high yet fluctuating abundance of *E. arctica* and *S. feylingi*, suggest ice marginal sea-ice conditions presumably in connection with enhanced incursion of drift ice loaded Polar Water conveyed by the EGC. The decreasing *C. neoteretis* and *I. norcrossi* point to relatively lower inflow of Atlantic derived waters to the shelf.

YD = Younger Dryas; HTM = Holocene Thermal Maximum). The blue bands mark periods influenced by relatively cold conditions, whereas red bands indicate time intervals of increased Atlantic Water advection.

6. Discussion

6.1. Deglacial-Holocene transition of the northeast Greenland shelf (13.3–11.1 cal ka BP, zone I)

The maximum extent of the GIS on the Northeast Greenland continental shelf during the last glaciation is somewhat contentious since data constraining the extent of the GIS during the last glaciation is scarce. Mass debris flows located at the slope adjacent to the shelf break together with glacial landforms observed across the shelf, indicate that during the Last Glacial Maximum (LGM) grounded glacial ice reached the shelf break (Arndt et al., 2017; Evans et al., 2009; Winkelmann et al., 2010). Yet, these landforms lack absolute dating. Marine sediment core PS2876 located at the North Greenland margin at 81 °N (Fig. 1a) records the onset of the deglaciation of the shelf at ~20 ka years BP, marked by a reduction in IRD and decreasing sedimentation rates (Nørgaard-Pedersen et al., 2008). Furthermore, a box core (PS93/031; Fig. 1a) retrieved at the Northeast Greenland continental margin at ~79° captures the late LGM period, during which Atlantic Water advection under perennial sea-ice conditions are evident (Spielhagen and Mackensen, 2021). Another new record (core DA17-NG-ST01-019G; Fig. 1a) from the outer NE Greenland shelf at 79.4 °N has been interpreted to show that grounded ice from the NEGIS never reached the shelf break at this site during the LGM. This interpretation is based on the presence of well-preserved macro and microfossils in radiocarbon dated marine sediments (Rasmussen et al., 2022).

Atlantic Water advection has been recorded in the deeper parts of the Fram Strait between c. 19.5 and 14.5 ka years BP, reaching as far north as ~78°N (Hebbeln et al., 1994). Additionally, high fluxes of planktonic foraminifera, high sedimentation rates and oxygen homogeneity between the western and eastern Fram Strait indicate an enhanced RAC during the LGM, which may have contributed to the retreat of the GIS (Nørgaard-Pedersen et al., 2003). This has recently been supported in the study of sediment core DA17-NG-ST01-019G from the NE Greenland shelf edge, where the rich planktonic and benthic foraminifera fauna point to relatively warm subsurface Atlantic water inflow during the LGM (Rasmussen et al., 2022).

In agreement with these observations, we hypothesize that the retreat of the grounded GIS occurred prior to c. 13.3 ka years BP at our study site. The high abundance of foraminiferal Atlantic Water indicator species and high planktonic foraminifera concentrations at the beginning of our record at c. 13.3 cal ka BP (Fig. 7a, c and Fig. 8d,g), imply advection of Atlantic Water masses to the Northeast Greenland shelf in line with the aforementioned studies. At the same time, the abundant, cold-water species *S. horvathi* suggests cold conditions (Figs. 7a and 8i). This was probably linked to increased influx of cold, low-saline surface meltwaters related to the rapid retreat of the nearby 79G in the Westwind Trough, which potentially yielded optimal conditions for sea-ice formation (Arndt et al., 2017).

According to the multiproxy study based on core PS100/270 retrieved east of 79G (Fig. 1a), the transition from grounded ice to ice free conditions is documented by a shift from subglacial till to laminated sediments (c. 10.1 cal ka BP) (Syring et al., 2020a); this is later than the assumed deglaciation at our core site. Thus, our study site on the middle section of the shelf was likely deglaciated earlier, as also in accordance with the more glacier proximal position of core PS100/270 (Syring et al., 2020a). In line with this, Norske Trough, located southwest of our core site, also appears to be free from grounded ice after c. 12.5 cal ka BP or even before 13.4 cal ka BP (core DA17-NG-ST08-092G, Fig. 1a) (Davies et al., 2022). The overall high IRD content, high sand content, low sedimentation rates, relatively high planktonic and calcareous benthic foraminifera fluxes and low *E. clavatum* in this zone at our core site might be indicative of ice rafting in a glaciomarine setting (Jennings et al., 2022) (Fig. 7d and e).

6.1.1. Bølling-Allerød interstadial (c. 13.3–12.9 cal ka BP)

The oldest part of core DA17-NG-ST03-039G encompasses the eastern Fram Strait timing of the Bølling-Allerød interstadial from 14.1 to 12.9 cal ka BP (Consolaro et al., 2018). During this time, a core from the deeper eastern Fram Strait records high sand and IRD content together with low surface water productivity (Consolaro et al., 2018) (Fig. 1a, Core JM10-330 GC). Additionally, a strong Atlantic Water inflow beneath Polar surface waters was inferred by high abundances of *C. neoteretis* (Consolaro et al., 2018). These conditions are commonly observed during the Bølling-Allerød in the eastern Fram Strait near the western Svalbard margin (Rasmussen et al., 2007; Ślubowska-Woldengen et al., 2007). Similarly, marine sediment cores from Southeast Greenland recorded increased advection of Atlantic Water during the Bølling-Allerød, starting at 13.5 cal ka BP (Jennings et al., 2006) (Fig. 1a core JM96-1216/2-GC). Overall, these studies align with our observations; high occurrences of *S. horvathi* and Atlantic Water indicator species together with relatively low abundance of *E. arctica* point to a stratified water column with increased Atlantic Water influence and low surface water productivity (Fig. 7a and b). Furthermore, the high IRD peak at c. 13.0 cal ka BP and high sand content might be indicative of ice rafting in a glaciomarine setting (Jennings et al., 2022) (Fig. 7d and e).

6.1.2. Younger Dryas (12.9–11.7 cal ka BP)

During the Younger Dryas (YD), a productivity bloom is recorded from c. 12.9 to 11.0 cal ka BP in core DA17-NG-ST03-039G, inferred by high Ca/Fe and high abundances of *E. arctica* and high planktonic and benthic foraminifera counts (Fig. 7b,c,g). The Atlantic Water indicator species decrease here. However, their persistently relatively high abundances indicate continued inflow of Atlantic Waters at subsurface levels. The Atlantic Water likely entered Westwind Trough below a cold and fresh surface meltwater layer, as inferred by continued high sand and IRD deposition at our core site, suggesting distal glaciomarine sedimentation. Glacial meltwater often delivers high concentrations of nutrients to the surrounding water masses, and thus may explain the observed productivity bloom recorded at our study site (Hopwood et al., 2018; Meire et al., 2017; Waniek et al., 2005). Yet, the high similarities between radiocarbon dates performed on planktonic and benthic foraminifera suggest overall well-ventilated water column conditions. Arndt et al. (2017) speculate that the fast flowing ice stream in the Westwind Trough was positioned at a mid shelf grounding zone wedge during the YD (Fig. 1b).

In line with our findings, core DA17-NG-ST-014-171G recovered offshore the Young Sound-Tyrolerfjord system in East Greenland (Fig. 1a), recorded extensive Atlantic Water advection leading to water column stratification during the YD (Jackson et al., 2022). Further to the south in Southeast Greenland, influence of Atlantic bottom waters also prevailed during the YD (12.8–11.64 cal ka BP) (core JM96-1216/2 GC, Fig. 1a), when the planktonic polar species *N. pachyderma* thrived (Jennings et al., 2006). This was likely due to enhanced injections of cold surface meltwater (Jennings et al., 2006). The strong ablation of the GIS in SE Greenland caused a $\delta^{18}O$ depletion in both the surface and bottom waters, despite a strong advection of Atlantic bottom waters inferred by high abundances of *C. neoteretis* (Jennings et al., 2006). Jennings et al. (2006) suggest that brine rejections related to sea-ice formation caused the surface waters to sink resulting in $\delta^{18}O$ bottom water depletion. A similar mechanism could have generated nutrient flux to the

bottom waters at our core site, causing a synchronous bloom in surface and bottom water productivity. Thus, the timing and the environmental conditions related to the YD observed in SE Greenland correlate with our observations (Fig. 7).

Relatively warmer conditions and/or no observed changes during the YD are in fact commonly observed around SE Greenland and Iceland, related to a continuous advection of Atlantic Waters (Eiríksson et al., 2000; Kuijpers et al., 2003) and it has also been traced to the Kane Basin off NW Greenland (Knudsen et al., 2008). In the eastern Fram Strait during the YD, several studies point to a persistent (yet colder and fresher) Atlantic water advection, beneath colder, sea-ice loaded Polar surface waters, caused by high summer melt rates and a strengthened Transpolar Drift (Aagaard-Sørensen et al., 2014b; Consolaro et al., 2018; Müller and Stein, 2014; Rasmussen et al., 2007; Ślubowska-Woldengen et al., 2007). Seasonal, pulsed primary production was linked to a bloom in opportunistic benthic foraminifera on the western Svalbard margin (Consolaro et al., 2018). A strong vertical water mass convection has also been observed in the first half of the YD in the central Fram Strait (core PS1230 Fig. 1a.) (Bauch et al., 2001).

At the Northeast Greenland continental slope (core PS93/031 Fig. 1a), low $\delta^{18}O$ values from *N. pachyderma* are recorded from 12.7 to 10.2 cal ka BP (Spielhagen and Mackensen, 2021). This suggests that a major freshwater event took place during parts of the YD, related to enhanced ablation of the GIS and/or connected to the freshwater outburst from the Mackenzie Valley into the Arctic Ocean (Spielhagen and Mackensen, 2021). Consequently, it has been suggested that the continuous ablation of the GIS and thus increased meltwater outflow during the Bølling-Allerød and YD yielded by a persistent advection of subsurface Atlantic Waters, could have played a role in the abrupt cooling event during the YD Holocene transition (Jennings et al., 2006; Rainsley et al., 2018).

6.1.3. The Early Holocene transition (11.7–11.1 cal ka BP)

Decreasing sand content and magnetic susceptibility together with variable Ca/Fe and Ca/Sr at around 11.7 cal ka BP marks the Holocene transition at our site, coinciding with rapidly increasing $\delta^{18}O$ values from the NGRIP ice core, suggesting overall transitional conditions (Figs. 5 and 7e,f,g). Variable Ca/Sr and Ca/Fe counts point to variations in the marine productivity and terrigenous influx. The end of the YD at 11.7 ka BP was associated with abrupt warming with mean annual air temperatures rising c. 10 °C in 60 years over the GIS (Steffensen et al., 2008; Walker et al., 2009). At our study site, this transition coincides with high percentages of Atlantic Water indicator species, indicative of warm intermediate water conditions (Figs. 7a and 8c).

After the onset of the Holocene, the increasing Ca/Fe and Ca/Sr after c. 11.4 cal ka point to increasing marine productivity (Fig. 5). The concurrent relatively high abundances of Atlantic Water indicator species suggest continuous advection of subsurface Atlantic Water (Figs. 7a and 8c). One large IRD peak at c. 11.1 cal ka BP (Figs. 6 and 8d), point to meltwater inflow associated with waning glaciomarine conditions potentially related to the final retreat of the NEGIS from the shelf (Larsen et al., 2018).

6.2. Variable mid-Holocene conditions and EGC strengthening (11.1–9.4 cal ka BP, zone II)

The Early to Mid Holocene environmental conditions on the Northeast Greenland shelf are characterized by significant fluctuations (Figs. 7 and 8). At c. 10.9 cal ka BP, the decreasing IRD, sand fraction percentages, sedimentation rate, Ca/Fe and Ca/Sr, *E. arctica*, calcareous benthic and planktonic fluxes are indicative of overall lower subsurface and surface productivity (Fig. 7). This could be related to reduced meltwater discharge in connection with a landward retreat of the nearby ice margin, and thus less supply of freshwater and nutrients to the water masses (Hopwood et al., 2018; Meire et al., 2017; Waniek et al., 2005).

From c. 11.1 to 10.2 cal ka BP the advection of Atlantic Water onto the shelf is strong given the continuous high percentages of Atlantic Water indicator species (Fig. 7a). The strong subsurface Atlantic Water advection is intermittently interrupted at 10.2 to 9.4 cal ka BP, recorded by the dominance of the opportunistic cold-water benthic species *E. clavatum* (Fig. 8m). *E. clavatum* indicates colder, fresher and unstable conditions potentially linked to a strong advection of EGC waters and/or waning glacial conditions (Syring et al., 2020a). Outside Young Sound (core DA17-NG-ST014-171G, Fig. 1a), seasonal sea-ice cover conditions and inflow of EGC Polar Water is also reported from c.10.9–8.8 cal ka BP (Jackson et al., 2022). Low $\delta^{13}C$ in *N. pachyderma* suggest poor ventilation related to cold surface water conditions and a reduced RAW advection at the neighbouring core site PS93/025 at c. 9.8 cal ka BP (Fig. 8f) (Zehnich et al., 2020).

6.3. Extensive sea-ice conditions and the Holocene thermal maximum (9.4–6.2 cal ka BP, zone III)

At c. 9.4 cal ka BP in our study, reduced sedimentation rates (Fig. 5) might point to source changes in terrigenous sedimentation. Concurrently, an increase in the percentages of *S. horvathi* and benthic productivity species (*S. feylingi*, *E. arctica*, and *N. labradorica*) that respond to pulses of primary productivity released from melting sea ice is observed (Fig. 8k); this might be linked to marginal ice zone conditions. This is supported by the concurrent maximum HBI III recorded in core PS93/025 (Figs. 1a and 8j) (Syring et al., 2020b). Syring et al. (2020a) and Zehnich et al. (2020) relate these sea-ice conditions and relatively low $\delta^{18}O$ in *C. neoteretis* to an overall warming of the surface and bottom waters (Fig. 8e). Signs of Atlantic Water advection to the grounding line of the 79G was also recorded in core PS100/270 from 10 to 9.6 cal ka BP (Fig. 1a) (Syring et al., 2020a). An abundance of ~12% of Atlantic Water indicator species in our study suggest some inflow of Atlantic Waters (Fig. 8c), potentially flowing beneath a Polar Water layer advected by a stronger EGC. Concurrently, a benthic foraminiferal record from Southeast Greenland report larger influence of the AAW together with a stronger expanded EGC in Denmark Strait (core JM96-1206/2 GC, Fig. 1a) (Perner et al., 2016) (Fig. 8b). Based on this, we hypothesize that the relatively abundant Atlantic Water indicators at our site at this time (Fig. 8c), was caused by a predominant influence of the AAW opposed to the RAW.

At 8.5 cal ka BP marginal sea-ice productivity is lower, inferred by decreasing percentages of the benthic productivity species that respond to the flux of food provided by the melting sea ice (Fig. 8k). This is related to generally lower IP_{25} and HBI III concentrations in core PS93/025, interpreted as low sea-ice algal productivity caused by an expansion of the sea-ice cover (Fig. 7i and j) (Syring et al., 2020b). This is also indicated by a peak in *S. horvathi* in our study, which tolerates heavy sea-ice conditions (Fig. 7l). Yet, the increasing abundance of the Atlantic Water indicator species at our site (Fig. 7c) suggests continuous inflow of Atlantic Water masses below an extended sea-ice cover. Contrasting water column conditions are also reported in the inner-trough area between Westwind and Norske Trough and on the inner Northeast Greenland continental shelf near the 79G, where *C. neoteretis* and *S. horvathi* co-existed (Pados-Dibattista et al., 2022 core DA17-NG-ST07-73G; (Syring et al., 2020a) core PS100/270, Fig. 1a). Near the site of 79G, these conditions were related to a proglacial environment with landfast sea ice, where a strong pycnocline separated the cold surface waters and the warm Atlantic-influenced subsurface waters (Syring et al., 2020b).

From 7.5 to 6.7 cal ka BP a strong incursion of subsurface Atlantic Water is inferred by increasing Atlantic Water indicators, reaching their highest abundances for the entire core. This marks the Holocene Thermal Maximum (HTM) at our site (Fig. 8c). The increasing $\delta^{13}C$ in *N. pachyderma* at that time in core PS93/025 point to enhanced water column ventilation (Fig. 8f)(Zehnich et al., 2020). Elevated abundances of the benthic productivity indicators and a high flux of planktonic foraminifera at our site (Fig. 8f,k), together with elevated concentrations of IP_{25} and HBI III in core PS93/025, suggest a transition towards marginal ice zone conditions with increased spring algal blooms (Fig. 8i and j) (Syring et al., 2020b). The strong advection of Atlantic Water might have caused sea-ice break-up on the outer shelf. Radiocarbon datings of whalebones and marine shells near the Nioghalvfjerdsfjorden at the 79G imply a reduction in the floating ice margin and prevailing open water conditions from 7.0 to 5.4 cal ka BP (Fig. 1b)(Bennike and Weidick, 2001; Larsen et al., 2018). Additionally, between 7.7 and 4.5 cal ka BP, the 79G grounding line was located 80 km inland compared to today (Bennike and Weidick, 2001).

On the inner Northeast Greenland shelf (core PS100/270, Fig. 1a), seasonal landfast sea ice was forming at the site of 79G in connection with the establishment of the Norske Øer Ice Barrier (NØIB) (Figs. 1b and 2) (Syring et al., 2020a). This was attributed to strong Atlantic Water incursion yielding enhanced basal melt of the glacier, destabilising the ice shelf. Rising of fresh, cold, less dense basal melt water acted as a barrier between the warm water, stabilizing the landfast sea-ice. Similarly, a strong influence of Atlantic Water, concurrent to a weakening of the EGC, is documented from c. 8.2 to 6.2 cal ka BP in the inter-trough area, related to the HTM (Pados-Dibattista et al., 2022; core DA17-NG-ST07-73G, Fig. 1a).

Seasonally-open water conditions in connection with reduced multiyear sea ice and landfast ice in Northern Greenland was also suggested by Funder et al. (2011a), based on the increased extent of beach ridges and sparse driftwood (Fig. 8h). These conditions were facilitated by atmospheric and ocean warming related to increased summer solar insolation during the HTM, where temperatures in the Arctic and North Greenland were 2 °C–4 °C warmer than today (Kaufman et al., 2004). This climatic warm period was also observed in marine records south of our study site, within the flow path of both the EGC and warmer Irminger Current (IC) at the North Icelandic Shelf. Here, a great influence of IC waters were recorded between c. 8.0 to 6.8 cal ka BP, related to the final phase of the HTM (Cabedo-Sanz et al., 2016; Ran et al., 2006). Closer to the SE Greenland margin in Denmark Strait, HTM conditions were marked by a strengthening and/or warming of the IC waters between c. 7.8–7.1 cal ka BP (Jennings et al., 2002, 2011; Perner et al., 2016) (Fig. 8a), whereas the AAW was the main contributor to the subsurface waters prior to 7.8 cal ka BP (Fig. 8b) (Perner et al., 2016). This is further supported by studies from the eastern Fram Strait near the WSC reporting strong inflow of Atlantic Water associated with the HTM until c. 7.0 cal ka BP (Consolaro et al., 2018; Rasmussen et al., 2014; Werner et al., 2013, 2016).

6.4. Onset of the neoglacial cooling (6.2–3.9 cal ka BP, zone IV)

From c. 6.2 to 3.9 cal ka BP, a weakening in the Atlantic Water inflow is inferred by decreasing abundance of the Atlantic Water indicator species at our site (Fig. 8c). Moreover, the planktonic flux and benthic productivity species peak around 6.3 cal ka BP followed by their sequent decrease (Figs. 6 and 8g). Opposite, the agglutinated benthic foraminiferal species are increasing in this zone. Altogether, this points to a transition towards colder subsurface and surface water conditions potentially linked to strong inflow of drift ice conveyed by the EGC interpreted from decreasing planktonic $\delta^{18}O$, HBI III and increasing IP_{25} in core PS93/025 (Fig. 8i and j) (Syring et al., 2020b; Zehnich et al., 2020). At the same time, the reappearance of driftwood in Northeast Greenland points to an increase in multiyear and landfast sea ice (Fig. 8h) (Funder et al., 2011a).

After the 79G ice shelf breakup at 7.5 cal ka BP, extremely low primary productivity, together with nearly permanent sea-ice cover, is observed at the inner NEG shelf (Davies et al., 2022; Syring et al., 2020a). This was followed by a re-advance of the 79G ice shelf from 4.5 cal ka BP, attributed to reduced Atlantic Water inflow slowing down the basal glacial melting (Bennike and Weidick, 2001; Syring et al., 2020a). Increased delivery of terrigenous sediment related to a readvance in the 79G ice shelf, might explain the increasing sedimentation rates (Fig. 6) (DA17-NG-ST03-039G). In the NEG mid-shelf region (core DA17-NG-ST07-073G, Fig. 1a), an initial cooling after the HTM is also dated to 6.2 cal ka BP (Pados-Dibattista et al., 2022). Although, here the most clear shift to colder conditions occurred at 4.2 cal ka BP, when there was a transition towards colder conditions associated with near perennial sea-ice cover conditions and an increased influx of Polar Water in the EGC (Pados-Dibattista et al., 2022). In fact, a general increase in EGC conveying drift ice along the east coast of Greenland starting from 4.7 to 3.3 cal ka BP is also reported by other studies in Denmark Strait and southeast Greenland (Andresen et al., 2013; Jennings et al., 2002; Perner et al., 2015b, 2016). Concurrently, the mussel *Mytilus edulis* vanished from East Greenland at 5 ka BP (Funder and Weidick, 1991; Hjort and Funder, 1974), suggesting cold conditions, as this species is commonly found in boreal-subarctic areas in Greenland (Dyke et al., 1996). Studies on driftwood, molluscs, marine mammal bones from raised marine deposits, together with lake and marine sediment cores from Northeast and East Greenland report on lower temperatures at around 5 cal ka BP and advancing glaciers (Bennike and Weidick, 2001; Klug et al., 2009; Syring et al., 2020a; Wagner et al., 2000).

Elevated abundances of Arctic diatom species recorded from 6.8 to 5.5 cal ka BP in a core retrieved from the North Icelandic Shelf within the flow path of the EGC supports this (Ran et al., 2006). Additionally, increases in *T. quinqueloba* and HBI III are recorded from 6.1 to 3.8 cal ka BP in core MD99-2269 (Harning et al., 2021) (Fig. 1a). Furthermore, elevated IP_{25} and quartz content are observed at c. 5 cal ka BP in both core MD99-2269 and JR51-GC35 on the North Icelandic Shelf (Cabedo-Sanz et al., 2016) (Fig. 1a). These observations indicate that the Arctic Front was positioned near the North Icelandic Shelf and that an expanded EGC conveyed drift ice from the Arctic Ocean to the area.

Evidence of colder conditions related to a weakening of the Atlantic Water inflow after 7 cal ka BP are also widespread in the eastern Fram Strait, based on several multiproxy studies off western Svalbard (Aagaard-Sørensen et al., 2014a; Aagaard-Sørensen et al., 2014b; Consolaro et al., 2018; Ebbesen et al., 2007; Rasmussen et al., 2014; Werner et al., 2013, 2016).

These Mid to Late Holocene cold conditions observed on the NEG shelf, North Icelandic Shelf, and Fram Strait region in other studies refer to the onset of the insolation-driven Neoglacial cooling, where the summer temperatures decreased gradually (Berger and Loutre, 1991; Berger, 1978; Kaufman et al., 2009). The timing of the onset of the Neoglaciation in the eastern Fram Strait appears to be more or less synchronous to that of the western Fram Strait, as several proxy studies document lower advection of Atlantic Waters parallel to a strengthening of the EGC and a south-eastward expansion of the sea-ice margin and Polar fronts (Aagaard-Sørensen et al., 2014b; Bauch et al., 2001; Belt and Müller, 2013; Consolaro et al., 2018; Hald et al., 2007; Harning et al., 2021; Koç et al., 1993; Rasmussen et al., 2007; Werner et al., 2013, 2016).

7. Conclusions

This study is the first to investigate the Last Glacial-Holocene transition and the general oceanographic development of the late glacial to Mid Holocene in the Westwind Trough, specifically in the area of the North East Water Polynya. Today, the site is influenced by cold, low-saline Polar Water of the upper EGC travelling from the Arctic Ocean underlain by warmer, saline Atlantic Water masses at subsurface levels. Our multiproxy study encompasses benthic foraminiferal assemblages, sediment properties and geochemical elemental composition (core scan data). Significant environmental variability is documented during the deglaciation and large part of the Holocene, related to relative fluctuations in sea-ice conditions, Atlantic and Polar Water influx (13.3–3.9 cal ka BP):

1. The Greenland Ice Sheet grounded ice had retreated from the outer Northeast Greenland shelf at 80°N by 13.3 cal ka BP, i.e. at least during the mid Bølling-Allerød period, where inflow of subsurface Atlantic Water below Polar surface waters and extensive sea-ice cover in a glaciomarine setting dominated the outer shelf. This was followed by increased productivity from c. 12.9 to 11.1 cal ka BP, derived by the highest abundances of *E. arctica* and the highest fluxes of both planktonic and benthic foraminifera together with high Ca/Fe and Ca/Sr ratios encompassing the timing of the YD.
2. Strong advection of Atlantic Water are recorded during the glacial-Holocene transition from c. 11.7 to 10.2 cal ka BP.
3. The period from 10.2 to 9.4 cal ka BP is characterized by enhanced incursion of cold Polar EGC Water and marginal ice zone conditions. This was followed by a period of harsher sea-ice conditions and inflow of subsurface Atlantic Water from c. 9.0 to 7.5 cal ka BP.
4. HTM related conditions are recorded from 7.5 to 6.7 cal ka BP, where the outer shelf was affected by increased productivity related to seasonal open water conditions and increased incursion of Atlantic-sourced water. The AAW may have been the main Atlantic Water source in the Westwind Trough during the HTM.
5. The shift towards a dominantly agglutinated fauna and lower abundance of benthic Atlantic Water indicator species at c. 6.2 cal ka BP points to a transition towards colder subsurface and bottom water conditions, potentially linked to the onset of the Neoglaciation. The decreased Atlantic Water incursion may have been facilitated by an enhancement of the EGC, conveying drift ice to the outer Northeast Greenland shelf.

Author contributions

Katrine Elnegaard Hansen: Writing - Original Draft, Writing - Review & Editing, Visualization, Data Curation, Investigation, Conceptualization, Formal analysis; Jesper Lorenzen: Formal analysis; Joanna Davies: Review & Editing; Lukas Wacker: Review & Editing, Formal analysis, Christof Pearce: Writing - Review & Editing, Supervision, Investigation, Resources, Conceptualization, Data Curation, Conceptualization, Visualization; Marit-Solveig Seidenkrantz: Writing - Review & Editing, Supervision, Funding acquisition, Investigation, Resources, Conceptualization, Data Curation, Cruise planning and Leading, Visualization.

Funding

The NorthGreen2017 expedition was funded by the Danish Centre for Marine Research and the Natural Science and Engineering Research Council of Canada. The research was funded by the Danish Council for Independent Research (grants no. 7014-00113B (G-Ice) and 0135–00165B (GreenShelf) to MSS), and by the iClimate Centre of Aarhus University, with additional funding from the European Union's Horizon 2020 research and innovation program under Grant Agreement No. 869383 (ECOTIP).

Declaration of competing interest

The authors declare that they have no known competing financial interests or personal relationships that could have appeared to influence the work reported in this paper.

Data availability

Benthic foraminiferal abundance data can be accessed at PANGAEA (https://doi.pangaea.de/10.1594/PANGAEA.943880).

Acknowledgements

We are grateful to the captain, crew and scientific party of the NorthGreen 2017 expedition on board *RV Dana*. We also wish to thank Trine Ravn-Jonsen (Aarhus University) for composing the X-Ray Fluorescence data set. We also thank Mimmi Oksman (GEUS) and Teodóra Pados-Dibattista (Aarhus University) for their assistance during core sampling and wet sieving. We warmly thank Katrine Juul Andresen (Aarhus University), Tove Nielsen (GEUS) and Tine L. Rasmussen (UiT the Arctic University of Norway) for site surveys. We also thank Hans Røy (Aarhus University), Anders Møller Mathiasen (Aarhus University) and Lasse Eriksen (Aarhus University) for core retrieval and Jørgen Bendtsen (Climate Lab, Copenhagen) and Søren Rysgaard (Arctic Research Centre, Aarhus University) for the CTD data. We are also grateful to Jochen Knies and an unnamed reviewer as well as to the editor Antje Voelker for their excellent suggestions and comments for improvement of the manuscript.

References

Aagaard, K., 1982. Inflow from the Atlantic Ocean to the polar basin. In: Rey, L. (Ed.), The Arctic Ocean: the Hydrographic Environment and the Fate of Pollutants. Palgrave Macmillan UK, London, pp. 69–81.

Aagaard, K., Coachman, L., 1968. The East Greenland current north of Denmark strait: part I. Arctic 21, 181–200.

Aagaard, K., Coachman, L., 1968. The East Greenland current north of Denmark strait: Part II. Arctic 21, 267–290.

Aagaard-Sørensen, S., Husum, K., Hald, M., Marchitto, T., Godtliebsen, F., 2014a. Sub sea surface temperatures in the Polar North Atlantic during the Holocene: planktic foraminiferal Mg/Ca temperature reconstructions. Holocene 24, 93–103. https://doi.org/10.1177/0959683613515730.

Aagaard-Sørensen, S., Husum, K., Werner, K., Spielhagen, R.F., Hald, M., Marchitto, T.M., 2014b. A late glacial-early Holocene multiproxy record from the eastern Fram Strait, polar North Atlantic. Mar. Geol. 355, 15–26. https://doi.org/10.1016/j.margeo.2014.05.009.

Aksu, A.E., 1983. Holocene and Pleistocene dissolutions cycles in deep-sea cores of Baffin Bay and Davis Strait: paleoceanographic implications. Mar. Geol. 53 (4), 331–348. https://doi.org/10.1016/0025-3227(83)90049-X.

Andresen, C.S., Hansen, M.J., Seidenkrantz, M.S., Jennings, A.E., Knudsen, M.F., Nørgaard-Pedersen, N., Larsen, N.K., Kuijpers, A., Pearce, C., 2013. Mid- to late-Holocene oceanographic variability on the Southeast Greenland shelf. Holocene. https://doi.org/10.1177/0959683612460789.

Arndt, J.E., Jokat, W., Dorschel, B., Myklebust, R., Dowdeswell, J.A., Evans, J., 2015. A new bathymetry of the Northeast Greenland continental shelf: constraints on glacial and other processes. Geochemistry, Geophysics, Geosystems 16 (10). https://doi.org/10.1002/2015GC005931.

Arndt, J.E., Jokat, W., Dorschel, B., 2017. The last glaciation and deglaciation of the Northeast Greenland continental shelf revealed by hydro-acoustic data. Quat. Sci. Rev. 160, 45–56. https://doi.org/10.1016/j.quascirev.2017.01.018.

Bahr, A., Lamy, F., Arz, H., Kuhlmann, H., Wefer, G., 2005. Late glacial to Holocene climate and sedimentation history in the NW Black Sea. Mar. Geol. 214, 309–322. https://doi.org/10.1016/j.margeo.2004.11.013.

Barber, D.G., Massom, R.A., 2007. Chapter 1 the role of sea ice in arctic and antarctic polynyas. Elsevier Oceanogr. Ser. 74, 1–54. https://doi.org/10.1016/S0422-9894(06)74001-6.

Bard, E., Tuna, T., Fagault, Y., Bonvalot, L., Wacker, L., Fahrni, S., Synal, H.A., 2015. AixMICADAS, the accelerator mass spectrometer dedicated to ^{14}C recently installed in Aix-en-Provence, France. Nucl. Instrum. Methods Phys. Res. Sect. B Beam Interact. Mater. Atoms 361, 80–86. https://doi.org/10.1016/j.nimb.2015.01.075.

Bauch, H.A., Erlenkeuser, H., Spielhagen, R.F., Struck, U., Matthiessen, J., Thiede, J., Heinemeier, J., 2001. A multiproxy reconstruction of the evolution of deep and surface waters in the subarctic Nordic seas over the last 30,000 yr. Quat. Sci. Rev. 20, 659–678. https://doi.org/10.1016/S0277-3791(00)00098-6.

Belt, S.T., Müller, J., 2013. The Arctic sea ice biomarker IP_{25}: a review of current understanding, recommendations for future research and applications in palaeo sea ice reconstructions. Quat. Sci. Rev. 79, 9–25. https://doi.org/10.1016/j.quascirev.2012.12.001.

Bennett, K.D., 1996. Determination of the number of zones in a biostratigraphical sequence. New Phytol. 132, 155–170. https://doi.org/10.1111/j.1469-8137.1996.tb04521.x.

Bennike, O., Weidick, A., 2001. Late Quaternary history around Niog-halvfjerdsfjorden and Jøkelbugten, North-east Greenland. Boreas 30 (3), 205–227. https://doi.org/10.1111/j.1502-3885.2001.tb01223.x.

Berger, A.L., 1978. Long-term variations of daily insolation and Quaternary Climatic Changes. J. Atmos. Sci. 35 (12), 2362–2367. https://doi.org/10.1175/1520-0469(1978)035<2362:ltvodi>2.0.co.

Berger, A., Loutre, M.F., 1991. Insolation values for the climate of the last 10 million years. Quat. Sci. Rev. 10 (4), 297–317. https://doi.org/10.1016/0277-3791(91)90033-Q.

Blott, S.J., Pye, K., 2001. Gradistat: a grain size distribution and statistics package for the analysis of unconsolidated sediments. Earth Surf. Process. Landforms 26, 1237–1248. https://doi.org/10.1002/esp.261.

Bourke, R.H., Newton, J.L., Paquette, R.G., Tunnicliffe, M.D., 1987. Circulation and water masses of the East Greenland shelf. J. Geophys. Res. Ocean. 92, 6723–6740. https://doi.org/10.1029/JC092iC07p06729.

Budéus, G., Schneider, W., Kattner, G., 1997. Distribution and exchange of water masses in the Northeast water polynya (Greenland sea). J. Mar. Syst. 10, 123–138. https://doi.org/10.1016/S0924-7963(96)00074-7.

Cabedo-Sanz, P., Belt, S.T., Jennings, A.E., Andrews, J.T., Geirsdóttir, Á., 2016. Variability in drift ice export from the Arctic Ocean to the North Icelandic Shelf over the last 8000 years: a multi-proxy evaluation. Quat. Sci. Rev. 146, 99–115. https://doi.org/10.1016/j.quascirev.2016.06.012.

Cage, A.G., Pieńkowski, A.J., Jennings, A., Knudsen, K.L., Seidenkrantz, M.-S., 2021. Comparative analysis of six common foraminiferal species of the genera *Cassidulina*, *Paracassidulina*, and *Islandiella* from the Arctic–North Atlantic domain. J. Micropalaeontol. 40, 37–60. https://doi.org/10.5194/jm-40-37-2021.

Consolaro, C., Rasmussen, T.L., Panieri, G., 2018. Palaeoceanographic and environmental changes in the eastern Fram Strait during the last 14,000 years based on benthic and planktonic foraminifera. Mar. Micropaleontol. 139, 84–101. https://doi.org/10.1016/j.marmicro.2017.11.001.

Croudace, I.W., Rindby, A., Rothwell, R.G., 2006. ITRAX: description and evaluation of a new multi-function X-ray core scanner. Geol. Soc. London, Spec. Publ. 267, 51–63.

Croudace, I.W., Löwemark, L., Tjallingii, R., Zolitschka, B., 2019. Current perspectives on the capabilities of high resolution XRF core scanners. Quat. Int. 514, 5–15. https://doi.org/10.1016/j.quaint.2019.04.002.

Davies, J., Mathiasen, A.M., Kristiansen, K., Hansen, K.E., Wacker, L., Alstrup, A.K.O., Munk, O.L., Pearce, C., Seidenkrantz, M.-S., 2022. Linkages between ocean circulation and the Northeast Greenland ice stream in the Early Holocene. Quat. Sci. Rev. 286. https://doi.org/10.1016/j.quascirev.2022.107530.

de Steur, L., Hansen, E., Mauritzen, C., Beszczynska-Möller, A., Fahrbach, E., 2014. Impact of recirculation on the East Greenland Current in Fram Strait: Results from moored current meter measurements between 1997 and 2009. Deep. Res. Part I Oceanogr. Res. Pap. 92, 26–40. https://doi.org/10.1016/j.dsr.2014.05.018.

Deser, C., Walsh, J.E., Timlin, M.S., 2000. Arctic sea ice variability in the context of recent atmospheric circulation trends. J. Clim. 13, 617–633. https://doi.org/10.1175/1520-0442(2000)013<0617:ASIVIT>2.0.CO, 2.

Dyke, A.S., Dale, J.E., McNeely, R.N., 1996. Marine Molluscs as Indicators of Environmental Change in Glaciated North America and Greenland during the Last 18 000 Years/Les mollusques marins et les changements du milieu dans la partie englacée de l'Amérique du Nord et du Groenland depuis 18 000 ans. Géogr. Phys. Quaternaire 50 (2), 125–184. https://doi.org/10.7202/033087ar.

Dyke, A.S., England, J., Reimnitz, E.R.K., Jette, H., 1997. Changes in Driftwood Delivery to the Canadian Arctic Archipelago : The Hypothesis of Postglacial Oscillations of the Transpolar Drift. Arctic 50 (1), 1–16. http://www.jstor.org/stable/40512037.

Ebbesen, H., Hald, M., Eplet, T.H., 2007. Lateglacial and early Holocene climatic oscillations on the western Svalbard margin, European Arctic. Quat. Sci. Rev. 26, 1999. https://doi.org/10.1016/j.quascirev.2006.07.020, 2011.

Eiríksson, J., Knudsen, K.L., Haflidason, H., Henriksen, P., 2000. Late-glacial and Holocene palaeoceanography of the north Icelandic shelf. J. Quat. Sci. 15, 23–42. https://doi.org/10.1002/(SICI)1099-1417(200001)15:1<23::AID-JQS476>3.0.CO;2-8.

El bani Altuna, N., Rasmussen, T.L., Ezat, M.M., Vadakkepuliyambatta, S., Groeneveld, J., Greaves, M., 2021. Deglacial bottom water warming intensified Arctic methane seepage in the NW Barents Sea. Commun. Earth Environ. 2, 188. https://doi.org/10.1038/s43247-021-00264-x.

Evans, J., Cofaigh, C.Ó., Dowdeswell, J.A., Wadhams, P., 2009. Marine geophysical evidence for former expansion and flow of the Greenland Ice Sheet across the north-east Greenland continental shelf. J. Quat. Sci. 24, 279–293. https://doi.org/10.1002/jqs.1231.

Farmer, J.R., Sigman, D.M., Granger, J., Underwood, O.M., Fripiat, F., Cronin, T.M., Martínez-García, A., Haug, G.H., 2021. Arctic Ocean stratification set by sea level and freshwater inputs since the last ice age. Nat. Geosci. 14, 684–689. https://doi.org/10.1038/s41561-021-00789-y.

Feyling-Hansen, R.W., Funder, S., 1990. Late Quaternary stratigraphy and glaciology in the Thule area, northwest Greenland. In: Funder, S. (Ed.), Fauna and Flora, Meddelelser Om Grønland, Geoscience, vol. 22. Kommissionen for Videnskabelige Undersøgelser i Grønland, Copenhagen, pp. 19–33.

Funder, S., Weidick, A., 1991. Holocene boreal molluscs in Greenland - palaeoceanographic implications. Palaeogeogr. Palaeoclimatol. Palaeoecol. 85 (1–2), 123–135. https://doi.org/10.1016/0031-0182(91)90029-Q.

Funder, S., Goosse, H., Jepsen, H., Kaas, E., Kjær, K.H., Korsgaard, N.J., Larsen, N.K., Linderson, H., Lysså, A., Möller, P., Olsen, J., Willerslev, E., 2011a. A 10,000-year record of Arctic Ocean sea-ice variability - view from the beach. Science 84 333, 747–751. https://doi.org/10.1126/science.1202760.

Funder, S., Kjeldsen, K.K., Kjær, K.H., O Cofaigh, C., 2011b. The Greenland Ice Sheet During the Past 300,000 Years: A Review. Dev. Quat. Sci. 15, 699–713. https://doi.org/10.1016/B978-0-444-53447-7.00050-7.

Grimm, E.C., 1987. CONISS: a FORTRAN 77 program for stratigraphically constrained cluster analysis by the method of incremental sum of squares. Comput. Geosci. 13, 13–35. https://doi.org/10.1016/0098-3004(87)90022-7.

Haine, T.W.N., Curry, B., Gerdes, R., Hansen, E., Karcher, M., Lee, C., Rudels, B., Spreen, G., de Steur, L., Stewart, K.D., Woodgate, R., 2015. Arctic freshwater export: Status, mechanisms, and prospects. Global Planet. Change 125, 13–35. https://doi.org/10.1016/j.gloplacha.2014.11.013.

Hald, M., Korsun, S., 1997. Distribution of modern benthic foraminifera from fjords of Svalbard, European Arctic. J. Foraminifer. Res. 27 (2), 101–122. https://doi.org/10.2113/gsjfr.27.2.101.

Hald, M., Steinsund, P.I., Dokken, T., Korsun, S., Polyak, L., Aspeli, R., 1994. Recent and late Quaternary distribution of *Elphidium excavatum* f. *Clavatum* in Arctic Seas. Cushman Found. Specieal Publ. 32, 141–153. ISBN electronic: 9781970168211.

Hald, M., Andersson, C., Ebbesen, H., Jansen, E., Klitgaard-Kristensen, D., Risebrobakken, B., Salomonsen, G.R., Sarnthein, M., Sejrup, H.P., Telford, R.J., 2007. Variations in temperature and extent of Atlantic Water in the northern North Atlantic during the Holocene. Quat. Sci. Rev. 26 (25–28), 3423–3440. https://doi.org/10.1016/j.quascirev.2007.10.005.

Hansen, B., Østerhus, S., 2000. North Atlantic-Nordic Seas exchanges. Prog. Oceanogr. 45, 109–208. https://doi.org/10.1016/S0079-6611(99)00052-X.

Harden, B.E., Pickart, R.S., Valdimarsson, H., Våge, K., de Steur, L., Richards, C., Bahr, F., Torres, D., Børve, E., Jónsson, S., Macrander, A., Østerhus, S., Håvik, L., Hattermann, T., 2016. Upstream sources of the Denmark Strait Overflow: observations from a high-resolution mooring array. Deep. Res. Part I Oceanogr. Res. Pap. 112, 94–112. https://doi.org/10.1016/j.dsr.2016.02.007.

Harning, D.J., Jennings, A.E., Köseoğlu, D., Belt, S.T., Geirsdóttir, Á., Sepúlveda, J., 2021. Response of biological productivity to North Atlantic marine front migration during the Holocene. Clim. Past 17, 379–396. https://doi.org/10.5194/cp-17-379-2021.

Hattermann, T., Isachsen, P.E., Von Appen, W.J., Albretsen, J., Sundfjord, A., 2016. Eddy-driven recirculation of Atlantic Water in Fram Strait. Geophys. Res. Lett. 43 (7), 3406–3414. https://doi.org/10.1002/2016GL068323.

Håvik, L., Pickart, R.S., Våge, K., Torres, D., Thurnherr, A.M., Beszczynska-Möller, A., Walczowski, W., von Appen, W.-J., 2017. Evolution of the East Greenland Current from Fram Strait to Denmark strait: Synoptic measurements from summer 2012. J. Geophys. Res. Ocean. 122 (3), 1974–1994. https://doi.org/10.1002/2016JC012228.

Heaton, T.J., Köhler, P., Butzin, M., Bard, E., Reimer, R.W., Austin, W.E.N., Bronk Ramsey, C., Grootes, P.M., Hughen, K.A., Kromer, B., Reimer, P.J., Adkins, J., Burke, A., Cook, M.S., Olsen, J., Skinner, L.C., 2020. Marine20 - The Marine Radiocarbon Age Calibration Curve (0-55,000 cal BP). Radiocarbon 62 (4), 779–820. https://doi.org/10.1017/RDC.2020.68.

Hebbeln, D., Dokken, T., Andersen, E.S., Hald, M., Elverhøi, A., 1994. Moisture supply for northern ice-sheet growth during the Last Glacial Maximum. Nature 370, 357–360. https://doi.org/10.1038/370357a0.

Hennekam, R., de Lange, G., 2012. X-ray fluorescence core scanning of wet marine sediments: methods to improve quality and reproducibility of high-resolution paleoenvironmental records. Limnol Oceanogr. Methods 10, 991–1003. https://doi.org/10.4319/lom.2012.10.991.

Higgins, A.K., 2015. Descriptive Text to the Geological Map of Greenland, 1:500 000, Lambert Land, Sheet 9, Geological Survey of Denmark and Greenland Map Series. https://doi.org/10.34194/geusb.v7.4563.

Hjort, C., Funder, S., 1974. The subfossil occurrence of *Mytilus edulis* L. in central East Greenland. Boreas 3 (1), 23–33. https://doi.org/10.1111/j.1502-3885.1974.tb00664.x.

Hopkins, T.S., 1991. The GIN Sea - A synthesis of its physical oceanography and literature review 1972-1985. Earth Sci. Rev. 30, 175–318. https://doi.org/10.1016/0012-8252(91)90001-V.

Hopwood, M.J., Carroll, D., Browning, T.J., Meire, L., Mortensen, J., Krisch, S., Achterberg, E.P., 2018. Non-linear response of summertime marine productivity to increased meltwater discharge around Greenland. Nat. Commun. 9. https://doi.org/10.1038/s41467-018-05488-8.

Husum, K., Hald, M., Stein, R., Weißschnur, M., 2015. Recent benthic foraminifera in the Arctic Ocean and Kara Sea continental margin. Arktos 5, 1–17. https://doi.org/10.1007/s41063-015-0005-9, 5.

Jackson, R., Andreasen, N., Oksman, M., Andersen, T.J., Pearce, C., Seidenkrantz, M.-S., Ribeiro, S., 2022. Marine conditions and development of the sirius water polynya on the north-east Greenland shelf during the younger dryas-holocene. Quat. Sci. Rev. 291. https://doi.org/10.1016/j.quascirev.2022.107647.

Jahn, A., Holland, M.M., 2013. Implications of Arctic sea ice changes for North Atlantic deep convection and the meridional overturning circulation in CCSM4-CMIP5 simulations. Geophys. Res. Lett. https://doi.org/10.1002/grl.50183.

Jennings, A.E., Helgadottir, G., 1994. Foraminiferal assemblages from the fjords and shelf of eastern Greenland. J. Foraminifer. Res. 24 (2), 123–144. https://doi.org/10.2113/gsjfr.24.2.123.

Jennings, A.E., Andrews, J.T., Knudsen, K.L., Hansen, C.V., Hald, M., 2002. A mid-Holocene shift in Arctic sea-ice variability on the East Greenland Shelf. Holocene 12, 49–58. https://doi.org/10.1191/0959683602hl519rp.

Jennings, A.E., Weiner, N.J., Helgadottir, G., 2004. Modern foraminiferal faunas of the southwestern to northern Iceland shelf: oceanographic and environmental controls. J. Foraminifer. Res. 34, 180–207. https://doi.org/10.2113/34.3.180.

Jennings, A.E., Hald, M., Smith, M., Andrews, J.T., 2006. Freshwater forcing from the Greenland ice sheet during the Younger Dryas: evidence from southeastern Greenland shelf cores. Quat. Sci. Rev. 25, 282–298. https://doi.org/10.1016/j.quascirev.2005.04.006.

Jennings, A., Andrews, J., Wilson, L., 2011. Holocene environmental evolution of the SE Greenland shelf north and south of the Denmark strait: Irminger and east Greenland current interactions. Quat. Sci. Rev. 30, 980–998. https://doi.org/10.1016/j.quascirev.2011.01.016.

Jennings, A., Andrews, J., Reilly, B., Walczak, M., Jakobsson, M., Mix, A., Stoner, J., Nicholls, K.W., Cheseby, M., 2020. Modern foraminiferal assemblages in northern Nares Strait, Petermann Fjord, and beneath Petermann Ice Tongue, NW Greenland. Arctic Antarct. Alpine Res. 52, 491–511. https://doi.org/10.1080/15230430.2020.1806986.

Jennings, A., Reilly, B., Andrews, J., Hogan, K., Walczak, M., Jakobsson, M., Stoner, J., Mix, A., Nicholls, K.W., O'Regan, M., Prins, M.A., Troelstra, S.R., 2022. Modern and early Holocene ice shelf sediment facies from Petermann Fjord and northern Nares Strait, northwest Greenland. Quat. Sci. Rev. 283, 107460. https://doi.org/10.1016/j.quascirev.2022.107460.

Juggins, S., 2020. rioja: Analysis of Quaternary Science Data. R package version 0.9-26. https://cran.r-project.org/package=rioja.

Kaufman, D.S., Ager, T.A., Anderson, N.J., Anderson, P.M., Andrews, J.T., Bartlein, P.J., Brubaker, L.B., Coats, L.L., Cwynar, L.C., Duvall, M.L., Dyke, A.S., Edwards, M.E., Eisner, W.R., Gajewski, K., Geirsdóttir, A., Hu, F.S., Jennings, A.E., Kaplan, M.R., Kerwin, M.W., Lozhkin, A.V., MacDonald, G.M., Miller, G.H., Mock, C.J., Oswald, W.W., Otto-Bliesner, B.L., Porinchu, D.F., Rühland, K., Smol, J.P., Steig, E.J., Wolfe, B.B., 2004. Holocene thermal maximum in the western Arctic (0-180°W). Quat. Sci. Rev. 23, 529–560. https://doi.org/10.1016/j.quascirev.2003.09.007.

Kaufman, D.S., Schneider, D.P., McKay, N.P., Ammann, C.M., Bradley, R.S., Briffa, K.R., Miller, G.H., Otto-Bliesner, B.L., Overpeck, J.T., Vinther, B.M., Abbott, M., Axford, Y., Bird, B., Birks, H.J.B., Bjune, A.E., Briner, J., Cook, T., Chipman, M., Francus, P., Gajewski, K., Geirsddttir, Á., Hu, F.S., Kutchko, B., Lamoureux, S., Loso, M., MacDonald, G., Peros, M., Porinchu, D., Schiff, C., Seppä, H., Thomas, E., 2009. Recent warming reverses long-term Arctic cooling. Science 84 325, 1236–1239. https://doi.org/10.1126/science.1173983.

Kleiber, H.P., Niessen, F., 2000. Variations of continental discharge pattern in space and time: implications from the Laptev Sea continental margin, Arctic Siberia. Int. J. Earth Sci. 89, 605–616. https://doi.org/10.1007/s005310000130.

Klenke, M., Schenke, H.W., 2002. A new bathymetric model for the central Fram Strait. Mar. Geophys. Res. 23, 367–378. https://doi.org/10.1023/A:1025764206736.

Klug, M., Bennike, O., Wagner, B., 2009. Repeated short-term bioproductivity changes in a coastal lake on Store Koldewey, northeast Greenland: an indicator of varying sea-ice coverage? Holocene, 19. https://doi.org/10.1177/0959683609104040.

Knudsen, K.L., Stabell, B., Seidenkrantz, M.S., Eiríksson, J., Blake, W., 2008. Deglacial and Holocene conditions in northernmost Baffin Bay: sediments, foraminifera, diatoms and stable isotopes. Boreas 37, 346–376. https://doi.org/10.1111/j.1502-3885.2008.00035.x.

Koch, L., 1945. The East Greenland Ice. Meddelelser fra Grønl. - Geosci. 130, 1–373.

Koç, N., Jansen, E., Haflidason, H., 1993. Paleoceanographic reconstructions of surface ocean conditions in the Greenland, Iceland and Norwegian seas through the last 14 ka based on diatoms. Quat. Sci. Rev. 12. https://doi.org/10.1016/0277-3791(93)90012-B, 1993.

Kuijpers, A., Troelstra, S.R., Prins, M.A., Linthout, K., Akhmetzhanov, A., Bouryak, S., Bachmann, M.F., Lassen, S., Rasmussen, S., Jensen, J.B., 2003. Late Quaternary sedimentary processes and ocean circulation changes at the Southeast Greenland margin. Mar. Geol. 195, 109–129. https://doi.org/10.1016/S0025-3227(02)00684-9.

Kwok, R., 2009. Outflow of Arctic Ocean Sea Ice into the Greenland and Barent Seas: 1979-2007. J. Clim. 22. https://doi.org/10.1175/2008JCLI2819.1.

Larsen, N.K., Levy, L.B., Carlson, A.E., Buizert, C., Olsen, J., Strunk, A., Bjørk, A.A., Skov, D.S., 2018. Instability of the Northeast Greenland Ice Stream over the last 45,000 years. Nat. Commun. 9, 3–10. https://doi.org/10.1038/s41467-018-04312-7.

Lloyd, J.M., 2006. Modern distribution of benthic foraminifera from Disko Bugt, West Greenland. J. Foraminifer. Res. 36, 315–331. https://doi.org/10.2113/gsjfr.36.4.315.

Locarnini, R.A., Mishonov, A.V., Baranova, O.K., Boyer, T.P., Zweng, M.M., Garcia, H.E., Reagan, J.R., Seidov, D., Weathers, K.W., Paver, C.R., Smolyar, I.V., 2019. World Ocean Atlas 2018, volume 1: temperature. A. Mishonov, technical editor. NOAA Atlas NESDIS 81, 52.

Marnela, M., Rudels, B., Houssais, M.N., Beszczynska-Möller, A., Eriksson, P.B., 2013. Recirculation in the Fram Strait and transports of water in and north of the Fram Strait derived from CTD data. Ocean Sci. 9, 499–519. https://doi.org/10.5194/os-9-499-2013.

Meire, L., Mortensen, J., Meire, P., Juul-Pedersen, T., Sejr, M.K., Rysgaard, S., Nygaard, R., Huybrechts, P., Meysman, F.J.R., 2017. Marine-terminating glaciers sustain high productivity in Greenland fjords. Global Change Biol. 23, 5344–5357. https://doi.org/10.1111/gcb.13801.

Morlighem, M., Williams, C.N., Rignot, E., An, L., Arndt, J.E., Bamber, J.L., Catania, G., Chauché, N., Dowdeswell, J.A., Dorschel, B., Fenty, I., Hogan, K., Howat, I., Hubbard, A., Jakobsson, M., Jordan, T.M., Kjeldsen, K.K., Millan, R., Mayer, L., Mouginot, J., Noël, B.P.Y., O'Cofaigh, C., Palmer, S., Rysgaard, S., Seroussi, H., Siegert, M.J., Slabon, P., Straneo, F., van den Broeke, M.R., Weinrebe, W., Wood, M., Zinglersen, K.B., 2017. BedMachine v3: Complete Bed Topography and Ocean Bathymetry Mapping of Greenland From Multibeam Echo Sounding Combined With Mass Conservation. Geophys. Res. Lett. 44 (21), 11,051–11,061. https://doi.org/10.1002/2017GL074954.

Mouginot, J., Rignot, E., Scheuchl, B., Fenty, I., Khazendar, A., Morlighem, M., Buzzi, A., Paden, J., 2015. Fast retreat of Zachariæ Isstrøm, northeast Greenland. Science 84 350, 1357–1361. https://doi.org/10.1126/science.aac7111.

Müller, J., Stein, R., 2014. High-resolution record of late glacial and deglacial sea ice changes in Fram Strait corroborates ice-ocean interactions during abrupt climate shifts. Earth Planet Sci. Lett. 403, 446–455. https://doi.org/10.1016/j.epsl.2014.07.016.

Müller, J., Werner, K., Stein, R., Fahl, K., Moros, M., Jansen, E., 2012. Holocene cooling culminates in sea ice oscillations in Fram Strait. Quat. Sci. Rev. https://doi.org/10.1016/j.quascirev.2012.04.024.

Nagler, T., Rott, H., Hetzenecker, M., Wuite, J., Potin, P., 2015. The Sentinel-1 Mission: New Opportunities for Ice Sheet Observations. Rem. Sens. 7, 9371–9389. https://doi.org/10.3390/rs70709371.

Nørgaard-Pedersen, N., Spielhagen, R.F., Erlenkeuser, H., Grootes, P.M., Heinemeier, J., Knies, J., 2003. Arctic Ocean during the Last Glacial Maximum: Atlantic and polar domains of surface water mass distribution and ice cover. Paleoceanography 18 (3). https://doi.org/10.1029/2002pa000781.

NASA, NASA Goddard Space Flight Center, Ocean Ecology Laboratory, Ocean Biology Processing Group, 2018. Moderate-resolution Imaging Spectroradiometer (MODIS) Aqua Inherent Optical Properties Data; 2018 Reprocessing. In: Greenbelt, M.D. (Ed.), Ocean Biology Processing Group. Moderate-Resolution Imaging Spectroradiometer (MODIS) Aqua Inherent Optical Properties Data; 2018. NASA OB.DAAC, USA doi:10.5067/AQUA/MODIS/L2/IOP/2018.

Nørgaard-Pedersen, N., Mikkelsen, N., Kristoffersen, Y., 2008. Late glacial and Holocene marine records from the Independence Fjord and Wandel Sea regions, North Greenland. Polar Res. 27 (2), 209–221. https://doi.org/10.1111/j.1751-8369.2008.00065.x.

NSIDC, 2020. Sea Ice Index, Version 3 [Data Set]. Boulder, Colorado USA. National Snow and Ice Data Center. https://doi.org/10.7265/N5K072F8. URL: https://masie_web.apps.nsidc.org/pub//DATASETS/NOAA/G02135/north/monthly/shapefiles/shp_median/.

Pados-Dibattista, T., Pearce, C., Detlef, H., Brendtsen, J., Seidenkrantz, M.-S., 2022. Holocene paleoceanography of the Northeast Greenland shelf. Clim. Past 18, 103–127. https://doi.org/10.5194/cp-18-103-2022.

Perner, K., Moros, M., Jennings, A., Lloyd, J.M., Knudsen, K.L., 2012. Holocene palaeoceanographic evolution off West Greenland. Holocene 23, 374–387. https://doi.org/10.1177/0959683612460785.

Perner, K., Moros, M., Lloyd, J.M., Jansen, E., Stein, R., 2015a. Mid to late Holocene strengthening of the East Greenland Current linked to warm subsurface Atlantic water. Quat. Sci. Rev. 129, 296–307. https://doi.org/10.1016/j.quascirev.2015.10.007.

Perner, K., Moros, M., Lloyd, J.M., Jansen, E., Stein, R., 2015b. Mid to late Holocene strengthening of the East Greenland Current linked to warm subsurface Atlantic water. Quat. Sci. Rev. https://doi.org/10.1016/j.quascirev.2015.10.007.

Perner, K., Jennings, A.E., Moros, M., Andrews, J.T., Wacker, L., 2016. Interaction between warm Atlantic-sourced waters and the East Greenland Current in northern Denmark Strait (68°N) during the last 10 600 cal a BP. J. Quat. Sci. 31, 472–483. https://doi.org/10.1002/jqs.2872.

Polyak, L., Korsun, S., Febo, L.A., Stanovoy, V., Khusid, T., Hald, M., Paulsen, B.E., Lubinsky, D.J., 2002. Benthic foraminiferal assemblages from the southern Kara Sea, a river-influenced Arctic marine environment. J. Foraminifer. Res. 32, 252–273.

Proshutinsky, A., Bourke, R.H., McLaughlin, F.A., 2002. The role of the Beaufort Gyre in Arctic climate variability: seasonal to decadal climate scales. Geophys. Res. Lett. 29, 2100. https://doi.org/10.1029/2002GL015847.

Rainsley, E., Menviel, L., Fogwill, C.J., Turney, C.S.M., Hughes, A.L.C., Rood, D.H., 2018. Greenland ice mass loss during the Younger Dryas driven by Atlantic Meridional Overturning Circulation feedbacks. Sci. Rep. 8, 1–9. https://doi.org/10.1038/s41598-018-29226-8.

Ramsey, C.B., 2008. Deposition models for chronological records. Quat. Sci. Rev. 27, 42–60. https://doi.org/10.1016/j.quascirev.2007.01.019.

Ramsey, C.B., Lee, S., 2013. Recent and planned developments of the program OxCal. Radiocarbon 55, 720–730. https://doi.org/10.1017/S0033822200057878.

Ran, L., Jiang, H., Knudsen, K.L., Eiríksson, J., Gu, Z., 2006. Diatom response to the Holocene climatic optimum on the North Icelandic shelf. Mar. Micropaleontol.

60, 226–241. https://doi.org/10.1016/j.marmicro.2006.05.002.
Rasmussen, S.O., Andersen, K.K., Svensson, A.M., Steffensen, J.P., Vinther, B.M., Clausen, H.B., Siggaard-Andersen, M.-L., Johnsen, S.J., Larsen, L.B., Dahl-Jensen, D., Bigler, M., Röthlisberger, R., Fischer, H., Goto-Azuma, K., Hansson, M.E., Ruth, U., 2006. A new Greenland ice core chronology for the last glacial termination. J. Geophys. Res. Atmos. 111. https://doi.org/10.1029/2005JD006079.
Rasmussen, T.L., Thomsen, E., Ślubowska, M.A., Jessen, S., Solheim, A., Koç, N., 2007. Paleoceanographic evolution of the SW Svalbard margin (76°N) since 20,000 ^{14}C yr BP. Quat. Res. 67, 100–114. https://doi.org/10.1016/j.yqres.2006.07.002.
Rasmussen, T.L., Pearce, C., Andresen, K.J., Nielsen, T., Seidenkrantz, M.-S., 2022. Northeast Greenland: ice-free shelf edge at 79.4°N around the Last Glacial Maximum 25.5–17.5 ka. Boreas. https://doi.org/10.1111/bor.12593.
Rasmussen, T.L., Thomsen, E., Skirbekk, K., Ślubowska-Woldengen, M., Klitgaard Kristensen, D., Koç, N., 2014. Spatial and temporal distribution of Holocene temperature maxima in the northern Nordic seas: interplay of Atlantic-, Arctic- and polar water masses. Quat. Sci. Rev. 92, 280–291. https://doi.org/10.1016/j.quascirev.2013.10.034.
Reimer, P.J., Reimer, R.W., 2001. A marine reservoir correction database and on-line interface. Radiocarbon 43, 461–463. https://doi.org/10.1017/s0033822200038339.
Reimer, P.J., Bard, E., Bayliss, A., Beck, J.W., Blackwell, P.G., Ramsey, C.B., Buck, C.E., Cheng, H., Edwards, R.L., Friedrich, M., Grootes, P.M., Guilderson, T.P., Haflidason, H., Hajdas, I., Hatté, C., Heaton, T.J., Hoffmann, D.L., Hogg, A.G., Hughen, K.A., Kaiser, K.F., Kromer, B., Manning, S.W., Niu, M., Reimer, R.W., Richards, D.A., Scott, E.M., Southon, J.R., Staff, R.A., Turney, C.S.M., van der Plicht, J., 2013. IntCal13 and Marine13 radiocarbon age calibration curves 0–50,000 Years cal BP. Radiocarbon 55, 1869–1887. https://doi.org/10.2458/azu_js_rc.55.16947.
Richter, T.O., Gaast, S. van der, Koster, B., Vaars, A., Gieles, R., de Stigter, H.C., de Haas, H., van Weering, T.C.E., 2006. The Avaatech XRF Core Scanner: technical description and applications to NE Atlantic sediments. Geol. Soc. London, Spec. Publ. 267, 39–50. https://doi.org/10.1144/GSL.SP.2006.267.01.03.
Richter, M.E., Von Appen, W.J., Wekerle, C., 2018. Does the East Greenland Current exist in the northern Fram Strait? Ocean Sci. 14, 1147–1165. https://doi.org/10.5194/os-14-1147-2018.
Rignot, E., Kanagaratnam, P., 2006. Changes in the velocity structure of the Greenland ice sheet. Science 80–. https://doi.org/10.1126/science.1121381.
Rothwell, R.G., Croudace, I.W., 2015. Twenty Years of XRF Core Scanning Marine Sediments: What Do Geochemical Proxies Tell Us? In: Croudace, I., Rothwell, R. (Eds.), Micro-XRF Studies of Sediment Cores. Developments in Paleoenvironmental Research, vol 17. Springer, Dordrecht. https://doi.org/10.1007/978-94-017-9849-5_2.
Rothwell, R.G., Hoogakker, B., Thomson, J., Croudace, I.W., Frenz, M., 2006. Turbidite emplacement on the southern Balearic Abyssal Plain (western Mediterranean Sea) during Marine Isotope Stages 1-3: an application of ITRAX XRF scanning of sediment cores to lithostratigraphic analysis. Geol. Soc. Spec. Publ. 267, 79–98. https://doi.org/10.1144/GSL.SP.2006.267.01.06.
Rudels, B., Jones, E.P., Anderson, L.G., Kattner, G., 1994. On the intermediate depth waters of the Arctic Ocean. In: Johannessen, O.M., Muench, R.D., Overland, J.E. (Eds.), The Polar Oceans and Their Role in Shaping the Global Environment. AGU, Washington, D. C., pp. 33–46. https://doi.org/10.1029/gm085p0033
Rudels, B., Korhonen, M., Budus, G., Beszczynska-Möller, A., Schauer, U., Nummelin, A., Quadfasel, D., Valdimarsson, H., 2012. The East Greenland Current and its impacts on the Nordic Seas: observed trends in the past decade. ICES J. Mar. Sci. 69 (5), 841–851. https://doi.org/10.1093/icesjms/fss079, 841–848.
Rysgaard, S., Vang, T., Stjernholm, M., Rasmussen, B., Windelin, A., Kiilsholm, S., 2003. Physical Conditions, Carbon Transport, and Climate Change Impacts in a Northeast Greenland Fjord. Arctic Antarct. Alpine Res. 35 (3), 301–302. https://doi.org/10.1657/1523-0430(2003)035[0301:PCCTAC]2.0.CO;2.
Rytter, F., Knudsen, K.L., Seidenkrantz, M.-S., Eiríksson, J., 2002. Modern distribution of benthic foraminifera on the north Icelandic shelf and slope. J. Foraminifer. Res. 32, 217–244. https://doi.org/10.2113/32.3.217.
Schaffer, J., von Appen, W.J., Dodd, P.A., Hofstede, C., Mayer, C., de Steur, L., Kanzow, T., 2017. Warm water pathways toward Nioghalvfjerdsfjorden Glacier, Northeast Greenland. J. Geophys. Res. Ocean. 122, 4004–4020. https://doi.org/10.1002/2016JC012462.
Schneider, W., Budéus, G., 1994. The North East Water Polynya (Greenland Sea). Polar Biol. 14, 1–9. https://doi.org/10.1007/BF00240265.
Seale, A., Christoffersen, P., Mugford, R.I., O'Leary, M., 2011. Ocean forcing of the Greenland Ice Sheet: calving fronts and patterns of retreat identified by automatic satellite monitoring of eastern outlet glaciers. J. Geophys. Res. Earth Surf. https://doi.org/10.1029/2010JF001847.
Seidenkrantz, M.-S., 1995. *Cassidulina teretis* Tappan and *Cassidulina neoteretis* new species (Foraminifera): stratigraphic markers for deep sea and outer shelf areas. J. Micropalaeontol. 14, 145–157. https://doi.org/10.1144/jm.14.2.145.
Seidenkrantz, M.S., 2013. Benthic foraminifera as palaeo sea-ice indicators in the subarctic realm - examples from the Labrador Sea-Baffin Bay region. Quat. Sci. Rev. 79, 135–144. https://doi.org/10.1016/j.quascirev.2013.03.014.
Seidenkrantz, M.-S., Andersen, J.R., Andresen, K.J., Bendtsten, J., Brice, C., Ellegaard, M., Eriksen, L.N., Gariboldi, K., Le Duc, C., Mathiasen, A.M., Nielsen, T., Ofstad, S., Pearce, C., Rasmussen, T.L., Ribeiro, S., Rysgaard, S., Røy, H., Scholze, C., Schultz, M., Wangner, D.J., 2018. NorthGreen2017 – a Marine Research Expedition to NE Greenland Onboard R/V *Dana*.
Ślubowska-Woldengen, M., Rasmussen, T.L., Koç, N., Klitgaard-Kristensen, D., Nilsen, F., Solheim, A., 2007. Advection of Atlantic Water to the western and northern Svalbard shelf since 17,500 cal yr BP. Quat. Sci. Rev. 26, 463–478. https://doi.org/10.1016/j.quascirev.2006.09.009.
Smedsrud, L.H., Halvorsen, M.H., Stroeve, J.C., Zhang, R., Kloster, K., 2017. Fram Strait sea ice export variability and September Arctic sea ice extent over the last 80 years. Cryosphere 11, 65–79. https://doi.org/10.5194/tc-11-65-2017.
Smith, R.S., Gregory, J.M., 2009. A study of the sensitivity of ocean overturning circulation and climate to freshwater input in different regions of the North Atlantic. Geophys. Res. Lett. 36 (15). https://doi.org/10.1029/2009GL038607.
Smith, S.D., Muench, R.D., Pease, C.H., 1990. Polynyas and leads: an overview of physical processes and environment. J. Geophys. Res. 95, 9461–9479. https://doi.org/10.1029/jc095ic06p09461.
Spielhagen, R.F., Mackensen, A., 2021. Upper ocean variability off NE Greenland (79°N) since the last glacial maximum reconstructed from stable isotopes in planktic foraminifer morphotypes. Quat. Sci. Rev. 265, 107070. https://doi.org/10.1016/j.quascirev.2021.107070.
Steffensen, J.P., Andersen, K.K., Bigler, M., Clausen, H.B., Dahl-Jensen, D., Fischer, H., Goto-Azuma, K., Hansson, M., Johnsen, S.J., Jouzel, J., Masson-Delmotte, V., Popp, T., Rasmussen, S.O., Röthlisberger, R., Ruth, U., Stauffer, B., Siggaard-Andersen, M.L., Sveinbjörnsdóttir, Á.E., Svensson, A., White, J.W.C., 2008. High-resolution Greenland ice core data show abrupt climate change happens in few years. Sci. 321, 680–684. https://doi.org/10.1126/science.1157707.
Stein, R., Nam, S. Il, Grobe, H., Hubberten, H., 1996. Late Quaternary glacial history and short-term ice-rafted debris fluctuations along the East Greenland continental margin. Geol. Soc. Spec. Publ. 111, 135–151. https://doi.org/10.1144/GSL.SP.1996.111.01.09.
Stein, R., Dittmers, K., Fahl, K., Kraus, M., Matthiessen, J., Niessen, F., Pirrung, M., Polyakova, Y., Schoster, F., Steinke, T., Fütterer, D.K., 2004. Arctic (palaeo) river discharge and environmental change: evidence from the Holocene Kara Sea sedimentary record. Quat. Sci. Rev. 23, 1485–1511. https://doi.org/10.1016/j.quascirev.2003.12.004.
Strass, V.H., Fahrbach, E., Schauer, U., Sellmann, L., 1993. Formation of Denmark Strait overflow water by mixing in the East Greenland Current. J. Geophys. Res. 98 (C4), 6907–6919. https://doi.org/10.1029/92jc02732.
Swingedouw, D., Braconnot, P., Marti, O., 2006. Sensitivity of the Atlantic Meridional Overturning Circulation to the melting from northern glaciers in climate change experiments. Geophys. Res. Lett. 33 (7). https://doi.org/10.1029/2006GL025765.
Syring, N., Lloyd, J.M., Stein, R., Fahl, K., Roberts, D.H., Callard, L., O'Cofaigh, C., 2020a. Holocene interactions between glacier retreat, sea-ice formation and Atlantic Water advection at the inner Northeast Greenland continental shelf. Paleoceanogr. Paleoclimatol. https://doi.org/10.1029/2020pa004019.
Syring, N., Stein, R., Fahl, K., Vahlenkamp, M., Zehnich, M., Spielhagen, R.F., Niessen, F., 2020b. Holocene changes in sea-ice cover and polynya formation along the eastern North Greenland shelf: new insights from biomarker records. Quat. Sci. Rev. 231, 106173. https://doi.org/10.1016/j.quascirev.2020.106173.
Topp, R., Johnson, M., 1997. Winter intensification and water mass evolution from yearlong current meters in the Northeast Water Polynya. J. Mar. Syst. 10 (1–4), 157–173. https://doi.org/10.1016/S0924-7963(96)00083-8.
Van Nieuwenhove, N., Limoges, A., Nørgaard-Pedersen, N., Seidenkrantz, M.-S., Ribeiro, S., 2020. Episodic Atlantic Water Inflow Into the Independence Fjord System (Eastern North Greenland) During the Holocene and Last Glacial Period. Front. Earth Sci. 8. https://doi.org/10.3389/feart.2020.565670.
Vare, L.L., Massé, G., Gregory, T.R., Smart, C.W., Belt, S.T., 2009. Sea ice variations in the central Canadian Arctic Archipelago during the Holocene. Quat. Sci. Rev. 28, 1354–1366. https://doi.org/10.1016/j.quascirev.2009.01.013.
Vilks, G., 1969. Recent Foraminifera in the Canadian Arctic. Micropaleontology 15 (1), 35–60. https://doi.org/10.2307/1484859.
Vilks, G., 1980. Postglacial Basin sedimentation on Labrador Shelf. Geological Survey of Canada Paper 78-28. https://doi.org/10.4095/106634.
Vinje, T.E., 1970. Sea ice observations in 1969. Arb. Nor. Polarinstitut 132–138.
Vinje, T., 1977. Sea ice conditions in the European sector of the marginal seas of the Arctic, 1966-1975. Nor. Polarinstitutt Årb. 1975 163–174.
Wacker, L., Fahrni, S.M., Hajdas, I., Molnar, M., Synal, H.-A., Szidat, S., Zhang, Y.L., 2013. A versatile gas interface for routine radiocarbon analysis with a gas ion source. Nucl. Instrum. Methods Phys. Res. Sect. B Beam Interact. Mater. Atoms 294, 315–319. https://doi.org/10.1016/j.nimb.2012.02.009.
Wadhams, P., 1981. The ice cover in the Greenland and Norwegian seas. Rev. Geophys. 19, 345–393. https://doi.org/10.1029/RG019i003p00345.
Wagner, B., Melles, M., Hahne, J., Niessen, F., Hubberten, H.W., 2000. Holocene climate history of Geographical Society Ø, East Greenland - evidence from lake sediments. Palaeogeogr. Palaeoclimatol. Palaeoecol. 160, 45–68. https://doi.org/10.1016/S0031-0182(00)00046-8.
Walker, M., Johnsen, S., Rasmussen, S.O., Popp, T., Steffensen, J.P., Gibbard, P., Hoek, W., Lowe, J., Andrews, J., Björck, S., Cwynar, L.C., Hughen, K., Kershaw, P., Kromer, B., Litt, T., Lowe, D.J., Nakagawa, T., Newnham, R., Schwander, J., 2009. Formal definition and dating of the GSSP (Global Stratotype Section and Point) for the base of the Holocene using the Greenland NGRIP ice core, and selected auxiliary records. J. Quat. Sci. 24, 3–17. https://doi.org/10.1002/jqs.1227.
Waniek, J.J., Holliday, N.P., Davidson, R., Brown, L., Henson, S.A., 2005. Freshwater control of onset and species composition of Greenland shelf spring bloom. Mar.

Ecol. Prog. Ser. 288, 45–57. https://doi.org/10.3354/meps288045.
Weatherall, P., Marks, K.M., Jakobsson, M., Schmitt, T., Tani, S., Arndt, J.E., Rovere, M., Chayes, D., Ferrini, V., Wigley, R., 2015. A new digital bathymetric model of the world's oceans. Earth Space Sci. 2 (8), 331–345. https://doi.org/10.1002/2015EA000107.
Werner, K., Spielhagen, R.F., Bauch, D., Hass, H.C., Kandiano, E., 2013. Atlantic Water advection versus sea-ice advances in the eastern Fram Strait during the last 9 ka: multiproxy evidence for a two-phase Holocene. Paleoceanography 28, 283–295. https://doi.org/10.1002/palo.20028.
Werner, K., Müller, J., Husum, K., Spielhagen, R.F., Kandiano, E.S., Polyak, L., 2016. Holocene sea subsurface and surface water masses in the Fram Strait – comparisons of temperature and sea-ice reconstructions. Quat. Sci. Rev. 147, 194–209. https://doi.org/10.1016/j.quascirev.2015.09.007.
Winkelmann, D., Jokat, W., Jensen, L., Schenke, H.W., 2010. Submarine end moraines on the continental shelf off NE Greenland - implications for Lateglacial dynamics. Quat. Sci. Rev. 29, 1069–1077. https://doi.org/10.1016/j.quascirev.2010.02.002.
Wollenburg, J.E., Mackensen, A., 1998. Living benthic foraminifers from the central Arctic Ocean: faunal composition, standing stock and diversity. Mar. Micropaleontol. 34, 153–185. https://doi.org/10.1016/S0377-8398(98)00007-3.
Wollenburg, J.E., Knies, J., Mackensen, A., 2004. High-resolution paleoproductivity fluctuations during the past 24 kyr as indicated by benthic foraminifera in the marginal Arctic Ocean. Palaeogeogr. Palaeoclimatol. Palaeoecol. 204, 209–238. https://doi.org/10.1016/S0031-0182(03)00726-0.
Yang, J., Luo, Z., Tu, L., 2020. Ocean Access to Zachariæ Isstrøm Glacier, Northeast Greenland, Revealed by OMG Airborne Gravity. J. Geophys. Res. Solid Earth 125 (11), e2020JB020281. https://doi.org/10.1029/2020JB020281.
Zehnich, M., Spielhagen, R.F., Bauch, H.A., Forwick, M., Hass, H.C., Palme, T., Stein, R., Syring, N., 2020. Environmental variability off NE Greenland (western Fram Strait) during the past 10,600 years. Holocene 30 (12), 1752–1766. https://doi.org/10.1177/0959683620950393.